Feature Extraction Methods for Palmprint Recognition: A Survey and Evaluation

Lunke Fei, *Member, IEEE*, Guangming Lu, Wei Jia, *Member, IEEE*, Shaohua Teng, and David Zhang, *Fellow, IEEE*

***Abstract*—Palmprint processes a number of unique features for reliable personal recognition. However, different types of palmprint images contain different dominant features. Instead, only some features of the palmprint are visible in a palmprint image, whereas the other features may not be notable. For example, the low-resolution palmprint image has visible principal lines and wrinkles. By contrast, the high-resolution palmprint image contains clear ridge patterns and minutiae points. In addition, the three dimensional (3-D) palmprint image possesses curvatures of the palmprint surface. So far, there is no work to summarize the feature extraction of different types of palmprint images. In this paper, we have an aim to completely study the feature extraction and recognition of palmprint. We propose to use a unified framework to classify palmprint images into four categories: 1) the contact-based; 2) contactless; 3) high-resolution; and 4) 3-D palmprint images. Then, we analyze the motivations and theories of the representative extraction and matching methods for different types of palmprint images. Finally, we compare and test the state-of-the-art methods via the widely used palmprint databases, and point out some potential directions for future research.**

***Index Terms*—3-D palmprint recognition, biometric, contact-based palmprint recognition, contactless palmprint recognition, high-resolution palmprint recognition.**

I. Introduction

BIOMETRICS refers to the use of distinctive anatomical and behavioral traits for automatically recognizing individuals [1]–[3]. With rapid development of e-commerce applications, such as Apple Pay, several biometric traits, including face, fingerprint, iris, ear, gait, and speech, have been studied and applied to the authentication of individuals [4]–[9]. As a relative new biometric trait, palmprint contains rich of intrinsic features, including the principal lines and wrinkles [3], and abundant ridge and minutiae-based features like a fingerprint [10]. These significant features of the palmprint are deemed to be permanent and unique to a subject [3], [10]. As a result, palmprint recognition has the potential to achieve high accuracy and reliable performance for personal verification and identification [11]–[15]. In addition, palmprint recognition, with high user-friendliness and easy self-positioning, is considered as a noninvasive biometric technology. Therefore, palmprint-based biometric has a wide range of potential usages for civilian and forensic applications [16]–[20].

To date, palmprint recognition has received increasing research attention, and a variety of methods have been proposed for palmprint feature extraction and recognition [3]–[30]. For example, Huang *et al*. [3] and Wu *et al*. [21] used the intrinsic features of palmprint, e.g., principal lines and wrinkles, for palmprint recognition. Yue *et al*. [22] proposed a hashing-based method for fast palmprint recognition. Roux *et al*. [23] proposed a phase-based method to improve the performance of the nonlinear deformed palmprint recognition. To further improve the performance of palmprint-based recognition, several multimodal-based palmprint recognition methods were proposed. Lin and Tai [24] proposed to combine the palmprint with palm vein and Xu *et al*. [25] fused both the left and right palmprint images for more accurate personal identification. Hong *et al*. [26] and Zhang *et al*. [27] studied the multispectral palmprint recognitions, which fused the features of palmprint images captured under a different spectrum. In addition, Kumar and Shekhar [28] investigated the rank-level fusion of multiple palmprint representations. Zhang *et al*. [30] provided a comparative study of palmprint recognition methods. Particularly, the currently popular deep-learning methods [17], [18] have also been applied in the field of palmprint recognition.

A. Features of Palmprint

It is known that palmprint features have multiple levels, and different levels of features are visible in different types of palmprint images. In general, the low resolution palmprint images, about 100 pixels per inch (ppi) [31], [32], are textured-based images, where the dark lines are the most significant and visible features. Of them, the top-three widest and longest lines are named principal lines and the other lines are

Manuscript received December 7, 2017; accepted January 11, 2018. Date of publication February 6, 2018; date of current version January 6, 2019. This work was supported in part by the National Natural Science Foundation of China under Grant 61702110 and Grant 61673175, and in part by the Guangzhou Science and Technology Program under Grant 201604046017 and Grant 201604030034. This paper was recommended by Associate Editor M. Celenk. *(Corresponding author: Lunke Fei.)*

L. Fei and S. Teng are with the School of Computer Science and Technology, Guangdong University of Technology, Guangzhou 510006, China (e-mail: flksxm@126.com; shteng@gdut.edu.cn).

G. Lu is with the Shenzhen Medical Biometrics Perception and Analysis Engineering Laboratory, Harbin Institute of Technology, Shenzhen 518055, China (e-mail: luguangm@hit.edu.cn).

W. Jia is with the School of Computer and Information, Hefei University of Technology, Hefei 230601, China (e-mail: icg.jiawei@gmail.com).

D. Zhang is with the Department of Computing, Biometrics Research Centre, Hong Kong Polytechnic University, Hong Kong 999077 (e-mail: csdzhang@comp.polyu.edu.hk).

Color versions of one or more of the figures in this paper are available online at http://ieeexplore.ieee.org.

Digital Object Identifier 10.1109/TSMC.2018.2795609

TABLE I
MAIN FEATURES IN DIFFERENT RESOLUTIONS OF PALMPRINT IMAGES

	Level-1(100 ppi)	Level-2 (500 ppi)	Level-3 (1000ppi)
Features	Principal lines; Wrinkles; Texture	Ridges; Valleys; Minutiae points; Creases	Pores; Ridge width

called wrinkles [33]. Thus, the principal lines, wrinkles and texture are the most dominant features of the low resolution palmprint images. Nevertheless, the ridges of the palmprint cannot be seen in the low-resolution palmprint images but are visible in the high-resolution palmprint images (about 500 ppi). Normally, the ridges form the basic features of the high-resolution palmprint images, including the ridge patterns (directions and densities), valleys, creases, and minutiae points [33]. Further, some local features of palmprint, such as pores, can only be detected in the very high-resolution palmprint images, that is more than 500 ppi or even 1000 ppi. Consequently, we group the palmprint features into three levels [10] as summarized in Table I.

B. Brief Review of Palmprint Recognition

Palmprint recognition refers to automatic identity authentication of a subject on a basis of one's unique features of palmprint. In general, lines are the most significant features of palmprint [21], and thus, the line-based methods play important roles in palmprint recognition. For example, Huang *et al*. [3] and Wu *et al*. [21] used the line features of palmprint images for personal authentication. However, using limited line features does not represent the uniqueness of palmprint images. To this end, a number of texture-based methods were proposed. Zhang *et al*. [32] proposed a palmcode method for online palmprint identification. Inspired by the palmcode, many orientation-based coding methods were proposed [34]–[38]. To broaden applications, a lot of recent works try to perform palmprint recognition under free conditions. In other words, the palmprint images are captured without restricting the placement of the hand [39]–[44], that is, the contactless palmprint images. The contactless palmprint images have serious variations on translations, scales, illuminations, and even suffer from noises. As a result, conventional methods are not very effective for contactless palmprint recognition. Therefore, additional features are usually exploited to improve the accuracy for contactless palmprint recognition [40]–[44]. For example, Morales *et al*. [40] and Wu *et al*. [44] extracted the scale invariant feature transform (SIFT) points from palmprint images to improve the performance of contactless palmprint verification.

Early palmprint recognition technologies focus on the low-resolution palmprint images, which are mainly used for the civil and commercial applications. However, high-resolution palmprint image-based recognition [33] is required for the high-security forensic applications, such as criminal detection. For example, statistics show that about 30% of the potential evidences recovered from crime scenes are from the high-resolution palmprint images [33]. It is known that the ridge-based features are the most significant and discriminative features of high-resolution palmprint images. The representative methods [47]–[50] usually extracted the minutiae points, including the ridge endings and bifurcates, and ridge patterns for reliable high-resolution palmprint recognition.

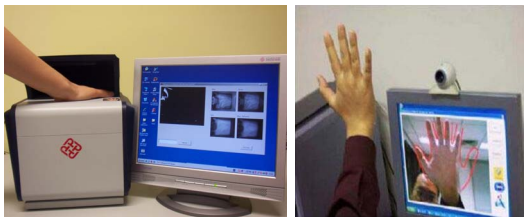

(a) (b)

Fig. 1. Two typical ways of palmprint image acquisition. (a) Principal way of contact-based palmprint image acquisition. (b) Typical model of contactless palmprint image acquisition.

With the advancements of three-dimensional biometrics, three-dimensional (3-D) palmprint recognition has received considerable concerns [51]–[57]. In 2008, Zhang *et al*. [52] designed a 3-D palmprint image acquisition device by using structured light technology, and established the first public 3-D palmprint database containing 8000 range data of 400 palm surfaces. Since then, various methods were proposed for 3-D palmprint recognition. Almost all methods [52]–[60] first calculated the mean curvature image (MCI) and Gaussian curvature image (GCI) of 3-D palmprint, and then extracted texture-based features. In addition, the surface type (ST) [58], which generally describes the structure types of a palm surface, was also calculated based on the signs of the curvatures in 3-D palmprint recognition.

C. Categories of Palmprint Images

It is believed that the palmprint recognition methods are associated with the characteristics of palmprint images. Thus, it is necessary to clarify the types of palmprint images before performing feature extraction and matching. In general, palmprint images can be classified based on different criteria. For example, based on the dimension of palmprint images, they can be grouped into the two-dimensional (2-D) and 3-D palmprint images [52]. According to the resolution, palmprint images can be divided into low-resolution and high-resolution palmprint images [32], [33]. In addition, the palmprint images can also be categorized based on the way of palmprint image acquisition, and thereby, they can be grouped into contact-based [40] and contactless palmprint images. The main difference of them is whether the hand is in contact with the acquisition device. Specifically, the former is captured with the palms placing on the device and the helps of user-pegs. By contract, the latter is collected with the hands do not touch the device. Fig. 1 shows two typical modes of the contact-based and contactless palmprint images acquisition [32], [61], respectively.

Existing works show that palmprint images can be divided into different groups according to different criteria. In this paper, we use a unified standard to group all kinds of palmprint images. We first categorize the palmprint images into 2-D and 3-D palmprint images, where the 2-D palmprint images

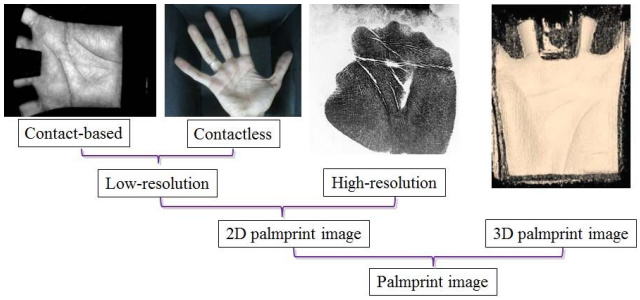

Fig. 2. Four categories of palmprint images, including the contact-based palmprint images, contactless palmprint images, high-resolution palmprint images, and 3-D palmprint images.

consist of the low-resolution and high-resolution palmprint images. Then, we group the low-resolution palmprint images into contact-based and contactless palmprint images. In general, both the high-resolution and 3-D palmprint images are the contact-based images. For simplicity, in this paper, the contact-based palmprint images and contactless palmprint images are specially referred to the low-resolution palmprint images. As a result, the palmprint images can be grouped into four categories, i.e., the contact-based, contactless, high-resolution, and 3-D palmprint images. Fig. 2 displays the classification of all kinds of palmprint images. It is seen that the palmprint images can be better grouped in the unified framework, and thus, the palmprint recognition methods can also be grouped based on the criteria.

D. Difference From Previous Works

Previous surveys on palmprint recognition usually focus on only one type of palmprint images. For example, both [19] and [22] comparatively study the palmprint recognition algorithms focusing only on the low-resolution palmprint images. In addition, Xinrong *et al*. [62] roughly divided the feature extraction methods into four categories and briefly review several methods for each category. However, it provides no clear standard for the classification of the feature extraction methods, and the motivations and theories of different methods are not analyzed. Also, it concentrates on the low-resolution palmprint recognition.

Existing works show that palmprint images have multiple categories, such as contactless palmprint images, high-resolution palmprint images, and 3-D palmprint images. Different types of palmprint images possess different dominant features and thus have different feature extraction methods. To the best of our knowledge, there is no work to systematically summarize the feature extraction and matching for all types of palmprint images. In this paper, we attempt to make such of the studies. We believe that this paper could provide researchers with a useful guideline working in the related fields.

E. Contributions of This Paper

The main contributions of this paper can be summarized as follows.

1) This paper groups palmprint images into four categories and provides a study of the feature extraction and recognition methods for all categories of palmprint images. Also, extensive experiments are conducted to compare and test the state-of-the-art palmprint recognition methods on the widely used palmprint databases.
2) We implement the popular deep-learning methods on contactless palmprint recognition, the results of which validate the effectiveness of the deep-learning methods on palmprint recognition.
3) We offer several potential research directions for palmprint recognition in the future.

F. Organization of This Paper

In this paper, we first group palmprint images into four categories based on a unified standard, and then study the principles of the representative feature extraction and recognition methods for each category. Furthermore, we compare and evaluate the state-of-the-art methods on the widely used palmprint databases and offer some potential research directions. Fig. 3 presents the organization of this paper.

The rest of this paper is organized as follows. Sections II–V review, analyze, and evaluate state-of-the-art methods of feature extraction and recognition for the contact-based palmprint images, contactless palmprint images, high-resolution palmprint images, and 3-D palmprint images. Section VI concludes this paper.

II. Contact-Based Palmprint Recognition

A. Features in Contact-Based Palmprint Image

Contact-based palmprint images contain visible line features. Of them, the most three longest and widest lines are the principal lines, that is, the heart line, head line, and life line [29], which are permanent for an individual. The other thinner and shorter lines are the wrinkles, which are mutable. Fig. 4 shows a typical contact-based palmprint image [63]. In addition, since the low-resolution palmprint images are texture-based images, the texture of contact-based palmprint images can also be considered as the significant features of them. Various local descriptors [64]–[68] were proposed by coding the texture features of palmprint images.

B. ROI

Before palmprint feature extraction, it is required to segment the region of interest (ROI) [32] of palmprint images. ROI is defined as a center part of a palmprint image. Several principles are designed to determine the ROI [69], [70]. The most common rule [32] of locating ROI is to set up the coordinate system based on the gap between fingers. Specifically, at first, the low-pass Gaussian filter is used to smooth the noise of the input palmprint image. Then, by directly thresholding, the smoothed palmprint image is converted into a binary image, based on which the boundary of the palmprint is detected using a boundary tracking algorithm. Third, the landmarks, which are at the bottom of gaps between index and middle fingers and between ring and little fingers, are located on the boundary as the reference points. Fourth, the perpendicular bisector of the line segment between two reference landmarks is set

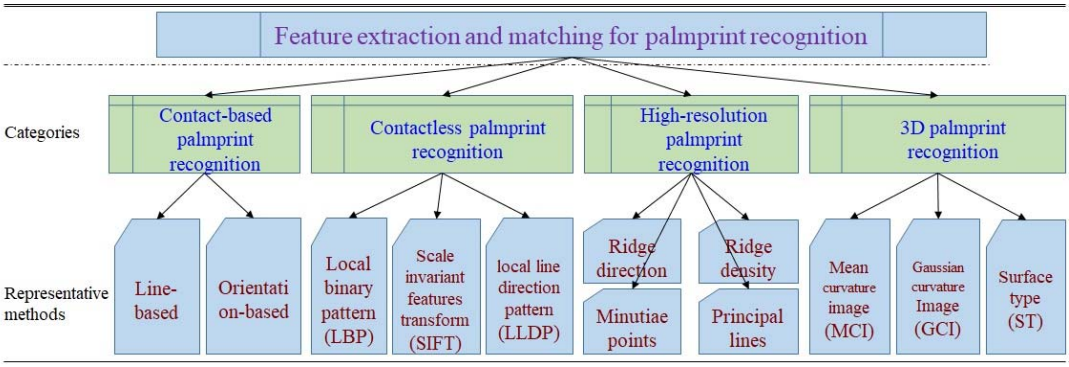

Fig. 3. Outline of this paper. It comprises four categories of palmprint recognition, including the contact-based, contactless, high-resolution, and 3-D palmprint recognition.

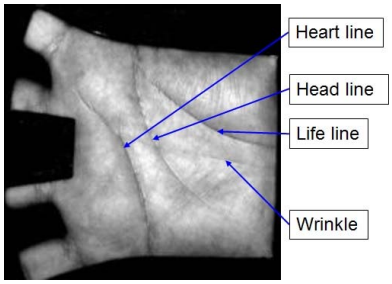

Fig. 4. Contact-based low-resolution palmprint image.

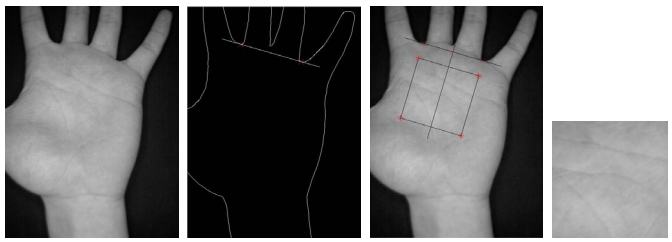

Fig. 5. Basic procedure of ROI extraction. (a) Input palmprint image. (b) Boundary of the palmprint image. (c) ROI location of the palmprint image. (d) Cropped ROI of the palmprint image.

up to find the location of ROI. Finally, the subimage at the certain area is cropped and resized, e.g., 128×128 pixels, as the ROI of the palmprint image. Fig. 5 shows the basic procedure of the ROI extraction. In general, palmprint images can be basically aligned after ROI extraction.

C. Feature Extraction of Contact-Based Palmprint Image

1) Line Features: Many algorithms were proposed to extract the line features for palmprint recognition [71]–[76]. The common rule of extracting line features is to use the line or edge detectors, including the difference of Gaussian filter (DoG) [30], Gabor filter [77]–[79], Radon filter [29], Sobel operation [71], and stack filter [80]. For example, in [30], it first defines a set of line detector filters based on first-order and second-order derivatives of a Gaussian function. Then, the palmprint image is convolved with these detectors. The lines in a palmprint can be detected by zero-crossing rule of the convolved results. Fig. 6 shows some examples [63] of palmprint lines extracted by using the line detectors described in [30]. It is noted that the DoG-based method [30] is sensitive to noise and illumination. In addition, the detected lines are too thin to distinguish the principal lines from wrinkles. As a result, the line-based method performs not good in palmprint recognition.

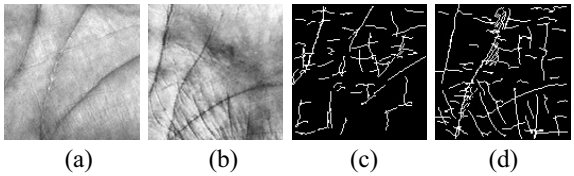

Fig. 6. (a) and (b) Two palmprint images and (c) and (d) corresponding line features of them.

The radon transform (RT) can detect the lines in an image by accumulating image intensity along all potential lines in an image. The original RT is usually performed on the image to detect all possible lines. Nevertheless, the lines in a palmprint image are generally existed in a limited local area. So the modified finite radon transform (MFRAT) [31] proposes to calculate the summation of image pixels over a set of lines in a certain area, which has the following general form:

$$r[L_k] = L_k \otimes (G \otimes I - I), (k = 1, 2, \ldots, N) \tag{1}$$

where I represents an input image, G is a Gaussian filter which is used to multiply the image and "$\otimes$" is the convolution operation. L represents a set of square templates preserving corresponding line structures and N is the number of the templates. Specifically, twelve line templates with orientations of $(k-1)\pi/12 (k = 1, 2, \ldots, 12)$ are usually used. Therefore, direction-map (D) and energy-map (E) of the palmprint image are, respectively, defined as follows:

$$D(i,j) = \arg\max_k \left(\left| r_{i,j}[L_k] \right| \right), (k = 1, 2, \ldots, N) \tag{2}$$

and

$$E(i,j) = \arg\max_r \left(\left| r_{i,j}[L_k] \right| \right), (k = 1, 2, \ldots, N) \tag{3}$$

where $|.|$ denotes the absolute value operation. Based on the energy image E, the line features can be directly detected by

(a) (b) (c)

Fig. 7. Palmprint images and corresponding line images. (a) Input ROI. (b) Principal line image. (c) Wrinkles extracted from the input ROI.

thresholding and thus the principal lines of a palmprint can be obtained by filtering out the small wrinkles under the energy criterion. By adjusting the threshold of the filtering criterion, the wrinkles can also be detected. Obviously, decreasing the threshold can detect more small wrinkles, otherwise, small wrinkles can be filtered out. Fig. 7 shows the typical principal line and wrinkle images extracted from an ROI [63] using the MFRAT [31] method.

Since the principal line map is binary, Hamming distance can be used for principal line matching. To overcome small misalignment, the pixel-to-area matching scheme [31] is more effective than the normal Hamming distance, which has the following form:

$$S(A,B)=\left(\sum_{i=1}^{m}\sum_{j=1}^{n}A(i,j)\cap\bar{B}(i,j)\right)\Big/N_A \tag{4}$$

where A and B are two principal line images, and $\bar{B}(i,j)$ represents a neighbor area of $B(i,j)$. N_A is the pixel number of principal lines in A. "$\cap$" represents the logical "AND" operation. The result of $A(i,j)\cap\bar{B}(i,j)$ is 1 if both $A(i,j)$ and at least one of $\bar{B}(i,j)$ are simultaneously in principal lines, otherwise, the result is 0.

The line features are insufficient to achieve high accuracy in palmprint recognition. As it is possible that some individuals have high similar principal lines [32]. Moreover, the wrinkles of palmprint images usually cannot be accurately extracted for they are sensitive to the noise and illumination changes.

2) Orientation-Based Features: Palmprint images are full of line and texture features which carry rich distinctive orientation information [81]. The local orientation-based descriptors can be exploited to represent the palmprint images. The representative orientation-based descriptors include the palmcode [32], competitive code [34], [82], fusion code [37], robust line orientation code method (RLOC) [31], double orientation code (DOC) [83], binary orientation co-occurrence vector (BOCV) [37], and E-BOCV [85] methods. In general, the orientation-based methods use one or multiple orientation-based templates to extract and encode the orientation features of palmprint [84], which has the following general procedure:

$$\text{Orientation\_code}(x,y)=\text{fun}(T(\theta)\otimes I(x,y)) \tag{5}$$

where $T(\theta)$ represents a template carries an orientation of θ, and I is a palmprint image. fun is a mapping function which encodes the convolved results into the orientation feature codes.

Originally, Zhang *et al*. [32] introduced a normalized 2-D Gabor filter to extract a spectral orientation ($\pi/4$) feature of

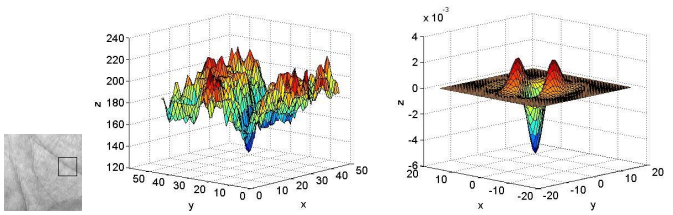

(a) (b) (c)

Fig. 8. Theory of the competitive code extraction. (a) Sub-image of the palmprint image with a clear line. (b) Intensity value distribution of the sub-image (a). (c) Gabor filter with a similar orientation as that of the line in (b).

palmprint images. Both the real and imaginary parts of the filter are convolved with a palmprint image and the convolved results are binarized into a pair of codes, which is named as palmcode. To extract the dominant orientation feature of a palmprint, Kong and Zhang [34] proposed a competitive code method by employing six Gabor filters with different orientations. The rule of dominant orientation extraction is based on the underlying assumption that the pixels in a palmprint image belong to a line. The filter response reaches the maximum when the orientation of one of the Gabor filters is consistent with the dominant orientation of a potential line in the palmprint image. Fig. 8 shows the basic idea of the dominant orientation extraction of the palmprint. It is not hard to deduce that the Gabor filter having the most similar orientation as the line feature can achieve the maximum filtering response, that is, the minimum convolved value, among all Gabor filters. Therefore, it is reasonable to treat the orientation of the Gabor filter as the orientation of the potential line.

The competitive code method [34] uses six orientations of $j\pi/6(j=0,1,\ldots,5)$ of Gabor templates to extract the most dominant orientation code of a palmprint based on the convolved result of them. The real part of Gabor filter has the following general form:

$$G(x,y,\theta,\mu,\sigma,\beta)=\frac{1}{2\pi\sigma\beta}\exp\left[-\pi\left(\frac{x'^2}{\sigma^2}+\frac{y'^2}{\beta^2}\right)\right]\cos\left(2\pi\mu x'\right) \tag{6}$$

where $x'=(x-x_0)\cos\theta+(y-y_0)\sin\theta$, $y'=-(x-x_0)\sin\theta+(y-y_0)\cos\theta$. (x_0,y_0) is the center of the function, μ is the radial frequency in radians per unit length, θ is the orientation of the Gabor filter in radians, and σ and β are the standard deviations of the elliptical Gaussian along x and y axis, respectively. The ranges of x and y are the sizes of the filter, e.g., 35×35 pixels. Six filters are convolved with the palmprint image, respectively, and the index of the orientation with the minimum convolved result is taken as the most dominant orientation code, that is, the competitive code of the palmprint. Suppose G_j is the real part of Gabor filter with orientation of $j\pi/6$, the competitive code of the palmprint image I is calculated as follows:

$$\text{CompCode}(x,y)=\arg\min_j\left(I(x,y)\otimes G_j\right). \tag{7}$$

The winner-take-all rule is widely used in dominant orientation extraction. For example, the fusion code method [35] used four complex Gabor filters with orientations of $j\pi/4(j=$

0, 1, 2, 3) to extract dominant orientation features of a palmprint. The RLOC [31] method extracted the principal orientation of a palmprint by using MFRAT. Xu *et al*. [86] proposed a more accurate dominant orientation representation method based on the maximum adding the second maximum Gabor filtering response. In addition, to represent the bend line directions of the palmprint images, Fei *et al*. [87] defined a bank of half-Gabor filters to extract the half-orientation features of the palmprint.

However, in real operation of dominant orientation extraction, the orientations of adopted filters are discrete. It is possible that none of the filter has the same orientation as the palmprint line. Using the single orientation of Gabor filter usually cannot get the correct dominant orientation feature of the palmprint. Actually, the dominant orientation of the palmprint image is related to two closed discrete orientations of Gabor filters. Motivated by this observation, Fei *et al*. [83] used DOCs to represent the dominant orientation feature of the palmprint.

Instead of extracting a single orientation feature, Guo *et al*. [37] proposed the BOCV method to encode all six orientation features of a palmprint. Further, Zhang *et al*. [85] improved the BOCV (E-BOCV) method by filtering out the fragile bits of BOCV with the thresholding rule. In addition, Fei *et al*. [88], [89] proposed the neighboring direction indicators (NDIs) and local multiple directional pattern (LMDP) methods to explore the relationships on neighboring orientations.

The winner-take-all rule can extract the most dominant orientation feature, which can better represent the line features of the palmprint and thus outperform other orientation-based methods. Among the dominant-orientation-based methods, the DOC method extracts two dominant orientation codes showing better robustness than the other methods extracting single orientation code. Among the multiple-direction-based methods, the E-BOCV is superior to the BOCV methods because it can filter out the unstable orientations of some points. In addition, the NDI and LMDP generally outperform both the dominant-orientation and multiple-orientation-based methods because they can adaptively represent the multiple dominant orientations of the palmprint.

The orientation-based methods generally represent a palmprint with one or more binary-based code planes. The Hamming distance can be the metric to evaluate the similarity of them [90], which has the following general form:

$$D(P,Q)=\frac{\sum_{k=1}^{K}\sum_{i=1}^{N}\sum_{j=1}^{N}(P_k(i,j)\oplus Q_k(i,j))}{K\times N^2} \tag{8}$$

where $P_k(Q_k)$ is the kth bit binary code plane and "$\oplus$" is the bitwise "exclusive OR" operation. N^2 is the size of the code plane and K is the number of the code planes.

3) OLOF: Differently from the conventional orientation-based methods, Sun *et al*. [36] proposed an orthogonal line ordinal feature (OLOF) method to represent palmprint image by exploring the ordinal distance of perpendicular orientations. OLOF shows better robustness to rotation and it is widely used in both contact-based and contactless palmprint recognition. So we specially review the OLOF method in this section. Specifically, three orthogonal line ordinal filters are designed by incorporating two 2-D Gaussian filters with perpendicular orientations and opposite phases. A normal 2-D Gaussian has the following formulation:

$$f(x,y,\theta)=\exp\left[-\left(\frac{x\cos\theta+y\sin\theta}{\delta_x}\right)^2-\left(\frac{-x\sin\theta+y\cos\theta}{\delta_y}\right)^2\right] \tag{9}$$

where $\delta_x(\delta_y)$ denotes the horizontal (vertical) scale of the of the Gaussian filter. Then, a general orthogonal line ordinal filter can be generated as follows:

$$OF(\theta)=f(x,y,\theta)-f(x,y,\theta+\pi/2) \tag{10}$$

where $\theta=\{0,\pi/6,\pi/3\}$. So the three ordinal filters are $OF(0)$, $OF(\pi/6)$, and $OF(\pi/3)$, respectively, which are convolved with a palmprint image and the sign of the convolved results are correspondingly encoded into binary codes, namely ordinal codes [36], [91].

D. Experiments

In this section, we conduct both palmprint verification and palmprint identification experiments to compare the performance of different methods on two public contact-based palmprint image databases. In experiments, both the representative line-based and orientation-based methods are implemented, including the principal line (PriLine) [29], competitive code (CompCode) [34], palmcode [32], fusion code (FusionCode) [35], ordinal code (OrdinalCode) [36], DOC [83], BOCV [37], E-BOCV [85], and RLOC [31] methods.

1) Contact-Based Palmprint Databases: The typical contact-based palmprint image databases include the PolyU and multispectral palmprint databases [63]. Of them, the PolyU database images are captured under normal visible illumination. The multispectral database images are captured under the red, green, blue, and near infrared (NIR) illuminations. In the following experiments, both the PolyU and multispectral databases are used.

The PolyU palmprint database [63] contains 7752 low-resolution palmprint images collected from 386 palms of 193 different individuals. Of them, 131 subjects were males and the other 62 were females. The youngest and oldest subjects were about 10 and 55 years old, respectively. All samples are captured in two sessions with an interval of about two months. In each session, around ten palmprint images were captured for each palm of an individual. Therefore, about 20 palmprint samples were acquired for an individual in two sections. It is pointed out that some subjects provided more or less than ten samples. For example, the 137th palm provided 17 images in the first session and the 150th palm provided only one image in the second session. Consequently, the PolyU palmprint database consists of 386 palms of images and each palm contains about 11 to 27 samples. The corresponding ROIs with the size of 128×128 pixels are also provided in the database. A typical ROI image from the PolyU database is presented in Fig. 9.

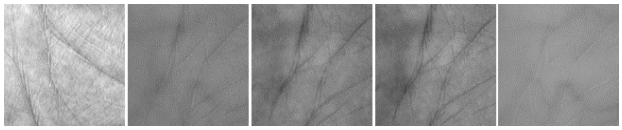

Fig. 9. Five palmprint image samples selected from the PolyU, M_Red, M_Green, M_Blue, and M_NIR palmprint databases.

The multispectral palmprint database [63] includes four independent spectral palmprint databases, namely Red, Green, Blue, and NIR palmprint databases. Specifically, 250 volunteers, including 195 males and 55 females, were asked to provide the palmprint images for both the left and right palms. The age distribution of them is from 20 to 60 years old. The images were collected in two separate sessions with the average time interval of 9 days. In each session, six images for each palm were captured under Red, Green, Blue, and NIR spectrum. Hence, four spectral palmprint databases were established, each of them contains 6000 images from 500 different palms and each palm has 12 images. Some typical palmprint ROI images of the multispectral databases are shown in Fig. 9. For convenience, in this paper, four spectral databases are referred as M_Red, M_Green, M_Blue, and M_NIR.

2) Palmprint Recognition Results: Palmprint verification [32] is a one-to-one comparison to verify that whether the two compared palmprint images are from the same palm or not. A comparison is called as a genuine match if the two palmprint images are from the same palm; otherwise, the comparison is considered an impostor match. In other words, the genuine match is an intraclass comparison and the impostor match is an interclass comparison. In the experiments, each palmprint image is compared with all other samples in the same database to get the genuine and impostor matching scores, respectively. After that, the equal error rate (EER), which is the point of false accept rate when it equals to false reject rate, is calculated as the basis of the evaluation [32]. In the PolyU database, the total number of matches is 30 042 876, of which 74 068 are genuine matches and 29 968 808 are impostor matches. In each of the multispectral databases, the total number of matches is 17 997 000, and the number of genuine matches and impostor matches are 33 000 and 17 964 000, respectively. For the sake of fair comparison, all algorithms are implemented on a PC with double-core Intel i5-3470 (3.2 GHz), RAM 8.00 GB, and MATLAB 8.3.0. Also, in this paper, all methods are conducted on the same platform unless otherwise stated. The EERs obtained using different methods are listed in Table II.

Palmprint identification [32] is the process of one-against-many comparisons to identify the class label of a query palmprint image. In experiments, some palmprint images per each palm are selected as the training images and the remaining palmprint images are used as the query samples. Specifically, for a database, the images captured in the first session are used as the training samples, and correspondingly, the images captured in the second session are used as the query samples. A query palmprint image will be compared with all training samples and classified into the class of the training sample which produces the highest similarity score with the query sample. The rank-1 identification error rates obtained based on different methods on the PolyU and four multispectral databases are summarized in Table III.

TABLE II
EERs (%) of Palmprint Verification Obtained Using Different Methods

	PolyU	M_Red	M_Blue	M_Green	M_NIR
PriLine	0.133	0.120	0.125	0.124	0.110
CompCode	0.026	0.015	0.017	0.017	0.014
Palmcode	0.093	0.030	0.051	0.050	0.033
FusionCode	0.090	0.018	0.022	0.021	0.021
OrdinalCode	0.027	0.016	0.020	0.020	0.018
DOC	0.019	0.012	0.015	0.014	0.012
BOCV	0.047	0.019	0.023	0.021	0.028
RLOC	0.049	0.022	0.025	0.020	0.021
E-BOCV	0.053	0.031	0.030	0.023	0.051

TABLE III
Error Rates (%) of the Palmprint Identification Obtained Using Different Methods

	PolyU	M_Red	M_Blue	M_Green	M_NIR
PriLine	9.02	9.90	10.69	11.13	10.29
CompCode	0.26	0.80	1.06	1.07	0.87
Palmcode	1.06	2.07	3.43	5.96	2.43
FusionCode	0.46	1.47	2.03	2.13	1.53
OrdinalCode	0.44	1.07	1.57	1.63	1.10
DOC	0.18	0.77	0.90	0.90	0.60
BOCV	0.28	1.63	1.83	1.80	1.80
RLOC	1.16	1.02	1.22	1.38	1.18
E-BOCV	0.76	1.50	1.23	1.57	1.90

From Tables II and III, we can draw the following findings. At first, the orientation-based methods perform much better than that of only using the line features. As orientation-based features have good discrimination and widely distributed in a palmprint. Comparatively, the principal lines of a palmprint are very limited and meanwhile many subjects possibly have similar principal lines. Second, the dominant orientation-based methods, including the competitive code and DOC methods, generally achieve higher accuracy than other methods. The possible reason is that the dominant orientation features can effectively represent the line features, which are the most significant and discriminative features of the palmprint. Further, the DOC achieves a higher accuracy than the other dominant orientation-based methods. The main reason is that the DOC method extracts DOCs to improve the robustness of the dominant orientation features of the palmprint. Comparatively, the palmcode method captures a certain but not dominant direction feature resulting to a low accuracy. Third, among dominant direction-based methods, the competitive code and DOC methods perform better than the RLOC method, which demonstrate that the Gabor template can better detect the orientation features of the palmprint than the MFRAT template. Fourth, the BOCV and E-BOCV methods also achieve competitive performance possibly because they can capture multiple orientation features of the palmprint. The main difference between them is that the E-BOCV method can detect and filter out the fragile orientation codes from the BOCV code map.

III. Contactless Palmprint Recognition

A. Feature Descriptors of Contactless Palmprint Image

Different from the contact-based palmprint images, the contactless palmprint images are taken with a commercial camera under free environments, where none user-peg is used to guide the placement of the hand in image acquisition [42]. So the contactless palmprint images are usually variant on rotations, translations, scales, illuminations and easily suffer from noise. Since the contactless palmprint images are low-resolution palmprint images, the lines and textures are also the most significant features of them. Because of misalignments and severe intraclass differences among contactless palmprint images, the conventional powerful palmprint recognition methods are not very effective in contactless palmprint recognition. A frequently used strategy to boost the accuracy of contactless palmprint recognition is to extract additional features from palmprint images [40]–[44]. In addition, the popular subspace learning approach [92] and collaborative representation [93] can also be attempted to the area of contactless palmprint recognition.

Because of the influence of the illumination, scale, rotation, and translation variances of contactless palmprint images, the features with high robustness should be useful for contactless palmprint recognition. Motivated by these observations, the SIFT [40] is frequently used in contactless palmprint recognition. Further, the local binary pattern (LBP) [94], [95], the local line directional patterns (LLDP) [96], and OLOF [36] show good robustness to rotation and illumination changes, and thus they can also be used in contactless palmprint recognition. Therefore, the robust features, such as SIFT, LBP, LLDP, and OLOF, can be considered as the significant features of contactless palmprint images. It is pointed out that the SIFT and LBP are not specially designed for representing palmprint images. Since these popular descriptors have been successfully used in contactless palmprint recognition, we briefly review them in this section.

B. Feature Extraction of Contactless Palmprint Image

1) SIFT: SIFT was originally proposed in [97] for object classification applications, which are introduced for contactless palmprint recognition achieving impressive performance [44]. The SIFT-based features are invariant to image scaling, rotation, and partially invariant to the changes of projection and illumination. So it is suitable to exploit the SIFT features for contactless palmprint images.

To extract the SIFT of the palmprint image, it first needs to establish the scale space of the sample by smoothing it with Gaussian template. Then, it searches over all scales and image locations by using a difference-of-Gaussian function to identify potential interest points of samples. Third, an elaborated model is used to determine finer location and scale at each candidate space and thus the key points are selected based on stability. Finally, the local image gradients are evaluated at the selected scale in the region around each key point to establish the direction histogram for each key point, and one or more main directions are assigned to the selected key points. Fig. 10 shows a typical example of SIFT-based features extracted from a contactless palmprint image [98]. In the matching stage, the Euclidean distance can be calculated to test the similarity between two SIFT descriptors.

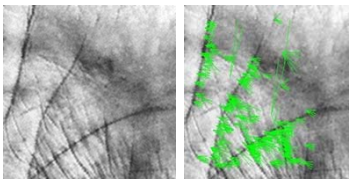

Fig. 10. SIFT features of a contactless palmprint image. (a) Contactless palmprint image ROI. (b) SIFT features of the palmprint image.

SIFT-based feature shows good robustness to rotation variations and scaling so that it is widely used in contactless palmprint recognition. For example, Wu *et al*. [44] proposed an SIFT-based contactless palmprint verification method. It first extracted the SIFT descriptors from contactless palmprint images and then removed the mismatched SIFT points based on the iterative RANSAC and local palmprint descriptor distance. The number of the final matched SIFT points is taken as the matching score of two samples in decision making. Zhao *et al*. [99] applied matched SIFT points to align the palmprint images, based on which the competitive codes are extracted. The matching scores of both the SIFT descriptors and competitive code planes are fused to improve the accuracy of contactless palmprint verification. In addition, SIFT can also be combined with other local orientation descriptors, such as OLOF [36].

2) LBP: LBP [94] is a simple yet powerful texture descriptor. It has high robustness to rotation and illumination changes and low computational complexity, which make it suitable for contactless palmprint recognition. LBP operator labels every pixel in an image by thresholding its neighboring pixels with the center value. The LBP is scale invariant since the differences between the center pixel with the neighboring pixels are not affected by changes in mean luminance. Fig. 11 illustrates an example to obtain the binary label for a pixel of an image in (8, 1) neighborhood. To achieve rotation invariance, an improved LBP mode can be obtained by bit-wise right shift on the original LBP bit string and the shifted string with the unique minimum value is selected as the rotation invariant LBP. Moreover, it is found that certain local binary patterns account for the fundamental information of texture, which are termed as "uniform" pattern. Supposing the LBP is a circular bit-wise string, the uniform pattern is the binary string that has at most two bitwise spatial transitions (bitwise 0/1 changes). In other words, the uniform patterns have the forms of "00000000" and "11111111" with no spatial transition, and "00111110" with two spatial transitions. To better represent the gray-scale and rotation invariant patterns, a number is given to describe each of the uniform patterns by summing up the number of "1" in it, and the "nonuniform" patterns are assigned to a certain number "$P + 1$," where P is the size of LBP. So the uniform pattern of the example in Fig. 11 is 5.

Based on LBP, Michael *et al*. [39] proposed a directional gradient with LBP (DGLBP) for contactless palmprint recognition. Specifically, four directional gradients of an input

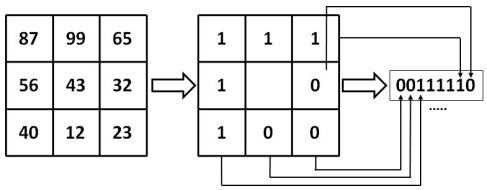

Fig. 11. Example of LBP.

palmprint image are calculated by using the Sobel operators with four directions, including the horizontal, vertical, diagonal at the 45 degree, and diagonal at the negative 45 degree. Each of gradient images is divided into nine equally sized sub-windows adding an overlapping center sub-window and the LBP is applied on each of sub-windows to extract the local texture feature. Finally, all sub-window LBP descriptors on four gradient images are concatenated to form the global descriptor of the image and the Chi-square [100] on the global descriptor is calculated at the feature comparison stage.

3) Local Directional Pattern: Inspired by LBP, local directional patterns (LDP) [101] is designed focusing on the image with rich of line features. LDP obtains eight-bit binary codes by comparing the edge responses of different directions in a local 3×3 neighborhood. Specifically, given a central pixel in an image, eight directional edge responses, e.g., $r_i (i = 0, 1, \ldots, 7)$, are calculated by convolving it with the Kirsch edge masks [101], which are a group of 3×3 templates containing different directional elements of "−3" and "5." The top k maximum responses are selected and corresponding directional bits are set to 1 and the remaining bits are set to 0. In other words, supposing r_k is the kth maximum filtering response, LDP code is derived by

$$\mathrm{LDP}_k = \sum_{i=0}^{7} s(r_i - r_k) 2^i \tag{11}$$

where $s(x)$ equals to 1 when $x \geq 0$, and 0 otherwise.

Extended by LDP, the enhanced LDP (ELDP) [102] is encoded based on the top- two maximum edge responses as $t_1 \times 8 + t_2$, where t_1 and t_2 are the directional index number of the top-two edge filtering responses. Local directional number (LDN) [99] encodes the LDP based on the maximum and minimum edge responses as $t_1 \times 8 + t_8$, where t_1 and t_8 denote the directional index number of the maximum and minimum edge responses, respectively. Supposing that the values in eight neighbors of Fig. 11 are the edge responses of eight directions, the top-three LDP, ELDP, and LDN of the center point are 14, 19, and 22, respectively.

Luo *et al.* [96] further extended LDP to LLDP to represent a palmprint image. Instead of using the gradient space, LLDP use the line directional space to extract the local line directional features. Specifically, the LLDP use the line filters, such as MFRAT and Gabor filters, with twelve orientations of $j\pi/12 (j = 0, 1, \ldots, 11)$ to convolve with a palmprint image. Then, the encode schemes of the LDP, EPLD, and LDN methods are, respectively, used to generate the LLDP-based descriptors.

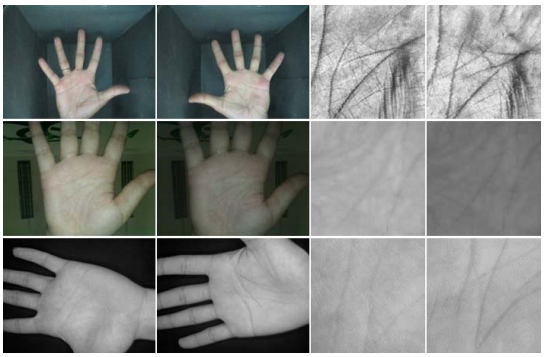

Fig. 12. Some typical contactless palmprint images. The first, second, and third rows present the original contactless palmprint images and corresponding ROIs of the IITD, GPDS, and CASIA databases, respectively.

C. Experiments

To compare the performances of different methods on contactless palmprint recognition, we carry out both palmprint verification and palmprint identification on widely used contactless palmprint image databases.

1) Contactless Palmprint Image Databases: The representative contactless palmprint image databases include IITD [98], GPDS [104], and CASIA [61] databases, which have been widely used to evaluate the effectiveness of contactless palmprint recognition methods. Thus, these three databases are used in this section.

The IITD database consists of 2600 contactless palmprint images collected from 460 palms of 230 different individuals. All the individuals in the database were in the age from 12 to 57 years old. In the palmprint images collection, each individual was asked to contribute five to six palmprint images for both the left and right palms. The palmprint images in the IITD database were captured by a camera in an indoor environment, where the hands are possibly variant in poses, projections, rotations, and translations. The first row of Fig. 12 shows some typical palmprint images and corresponding ROIs of the IITD database.

The GPDS database contains 1000 images collected from the right hands of 100 subjects, each of which provided ten palmprint images. All the palmprint images in the database were captured in a single session with uncontrolled background and illumination. The second row of Fig. 12 shows two typical palmprint images and corresponding ROIs of the GPDS database, where the surrounding illumination are obviously changed.

The CASIA database contains over 5500 palmprint images collected from 312 subjects. Eight to 17 palmprint images were captured from both the left and right palms for an individual. Also, there was no guideline on the posture and position placement of the hands in image acquisition. So the palmprint images generally have significant variations on postures, positions, and scales. As the ROIs are not provided in the CASIA database. We crop the ROIs of the palmprint images using the algorithm described in Section II. The third row of Fig. 12 shows two typical palmprint images of the CASIA database and the corresponding ROIs.

2) Palmprint Recognition Results: We compare the performance of state-of-the-art methods on both palmprint verification and palmprint identification in terms of EER and error rate, respectively. Several representative contactless palmprint recognition methods, including SIFT_OLOF [40], DGLBP [39]. SIFT_IRANSAC_OLOF [44], LLDP [96], are compared in the experiments. For the LLDP method, both MFRAT and Gabor filters are used to obtain the line orientation feature, respectively, and then the LDN coding scheme is used. The LLDP descriptors obtained by the MFRAT and Gabor filter are referred to LLDP_MFRAT and LLDP_Gabor, respectively. To test the effectiveness of the contact-based methods contactless palmprint recognition, we also implement conventional state-of-the-art palmprint recognition methods in the experiments. Specifically, we select two typical dominant-orientation-based methods, including the competitive code and DOC methods, and two representative multiple-orientation-based methods, including the ordinal code and E-BOCV methods, for contactless palmprint recognition.

It is seen that contactless palmprint images usually suffer from serous misalignment and influence of noise. The conventional binary code-based methods possibly cannot achieve comparable performance in contactless palmprint recognition. In addition, large-scale biometric image recognition has appeared to be an important direction in real-world applications. Existing works show us that the deep-learning-based methods have achieved promising performance in the computer vision and pattern recognition community, especially for large-scale image-based recognition. To explore more potential and feasible approaches for the challenging contactless palmprint recognition, we implement state-of-the-art deep-learning methods for contactless palmprint identification for better comparison, as well as validating the effectiveness of the deep-learning methods on the palmprint recognition.

The compared deep-learning methods include AlexNet [105], VGG-16 [106], Inception-V3 [107], and ResNet-50 [108]-based methods. Of them, the AlexNet contains eight learned, five convolutional, and three fully connected layers. A 1000-way softmax connected with the fully connected layer produces the classification results. The ReLU nonlinearity is used to the output of every convolutional and fully connected layers. Comparatively, VGG-16 comprises five pooling layers and 13 convolutional layers with the small filter sizes of 3×3. All hidden layers are equipped with ReLU nonlinearity. In addition, ResNet-50 with similar architecture as the conventional networks contains shortcut connections to each 3-layer of 3×3 filters. Inception-V3 introduces the BN and gradient clipping to scale up convolution networks, and also it adds label-smoothing regularization layer under the full-connected layer. These deep-learning methods are implemented on a PC with Inter Core i7-2600 CPU@3.40 Hz, graphics card of GTX1080 8G and RAM of 16 G (1333 MHz). The software is based on Python 2.7, CUDA 8.0, Cudnn 5.0, and the framework is based on MXNet (the version of MXNet is mexnet-0.11).

In the palmprint identification, we select the first four images per each palm as the training samples and use the rest images as the query samples. All models are first pretrained on the ImageNet [109] database. Then, we further train each model with fine-tuning based on the corresponding gallery sets selected from each palmprint database.

TABLE IV
EERs (%) OBTAINED USING DIFFERENT METHODS IN CONTACTLESS PALMPRINT VERIFICATION

	IITD	GPDS	CASIA
CompCode	0.101	0.396	0.075
OrdinalCode	0.109	0.413	0.078
DOC	0.062	0.492	0.072
E-BOCV	0.089	0.510	0.064
SIFT_OLOF	0.074	0.288	0.062
DGLBP	0.132	0.340	0.071
SIFT_IRANSAC_OLOF	0.074	0.279	0.059
LLDP_MFRAT	0.031	0.294	0.030
LLDP_Gabor	0.028	0.242	0.029

TABLE V
ERROR RATES (%) OBTAINED USING DIFFERENT METHODS IN CONTACTLESS PALMPRINT IDENTIFICATION

	IITD	GPDS	CASIA
CompCode	22.21	13.97	20.73
OrdinalCode	26.68	14.47	26.74
DOC	10.01	18.92	21.49
E-BOCV	14.07	12.84	15.94
SIFT_OLOF	10.56	12.36	10.01
DGLBP	23.56	29.21	21.32
SIFT_IRANSAC_OLOF	6.72	9.83	8.54
LLDP_MFRAT	7.25	9.55	9.23
LLDP_Gabor	4.83	5.87	7.00
AlexNet	11.82	9.50	5.09
VGG-16	7.88	8.67	5.99
Inception-V3	3.78	4.69	6.15
ResNet-50	4.43	6.09	4.79

The comparative results, including the EER of the palmprint verification and the error rate of rank-1 palmprint identification, are summarized in Tables IV and V, respectively. From above tables, we can obtain the following findings. At first, both the SIFT_OLOF and SIFT_IRANSAC_OLOF methods perform better than the ordinal method validating the effectiveness of the SIFT on contactless palmprint recognition. Second, LLDP-based methods, including both LLDP_MFRAT and LLDP_Gabor, achieve much higher accuracy than the LBP-based method. The main reason is that the LLDP-based methods are especially designed based on the palmprint line directions, which are the most significant and discriminative features of the palmprint. Third, the LLDP_Gabor achieves a better accuracy than the LLDP_MFRAT. Possibly because the Gabor filter can better characterize the line features of the palmprint images than the MFRAT filter.

The comparative results also show that the conventional methods, such as the competitive code, DOC, ordinal code, and E-BOCV methods, cannot achieve as high accuracy as that on contact-based palmprint recognition. The possible reason is the significant variances of contactless palmprint images on translation, rotation, and illumination, as well as of relatively low quality, and thus the conventional methods generally cannot stably and robustly capture the orientation features of contactless palmprint images. Also, the overall accuracy of contactless palmprint recognition is lower than that of contact-based

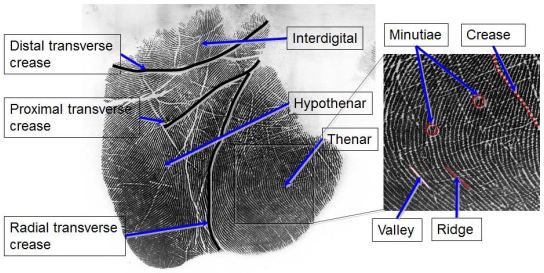

Fig. 13. Typical high-resolution palmprint image.

palmprint recognition. However, in real-world applications, contactless palmprint recognition is easily acceptable due to its high user-friendliness. Therefore, it is meaningful to further develop the contactless palmprint recognition to boost the accuracy. It is seen that the deep-learning methods can achieve comparable or even better performance than the conventional palmprint recognition methods, which provide us a new direction that investigating the deep-learning-based palmprint recognition technology. In the future, how to combine the conventional technology with the deep-learning appears to be an interesting and meaningful direction of contactless palmprint recognition. In addition, increasing the robustness of contactless palmprint recognition method is still the main research direction, and also how to automatically and accurately extract the ROI from contactless palmprint images is another challenging problem.

IV. High-Resolution Palmprint Recognition

A. Features in High-Resolution Palmprint Image

High-resolution palmprint images are resolutions of greater than 400 ppi [33] and have visible palmer friction ridges and palmer friction creases. Palmer friction ridges are the corrugated skin patterns and palmer friction creases are discontinuities of the ridge patterns. Fig. 13 shows a typical high-resolution palmprint image [110], where the dark lines are the ridges and the white lines are valleys and creases of the palmprint. The ridge endings and bifurcates constitute the minutiae points of the palmprint [33]. Among the friction creases, three longest creases are the principal lines, which are named as distal transverse crease, proximal transverse crease, and radial transverse crease, respectively. The principal lines divide the palmprint into three regions, namely, interdigital, hypothenar, and thenar, which are denoted in Fig. 13.

B. Feature Extraction of High-Resolution Palmprint Image

1) Local Ridge Direction: Local ridge direction (LRD) [10], [33] is associated with the pixels of the palmprint images. LRD at a pixel is defined as the angle between the ridge crossing through an arbitrary small neighborhood area of the pixel and the horizontal axis. LRD can be represented as $(\theta_{i,j}, r_{i,j})$, where $\theta_{i,j}$ is the ridge direction of the (i, j) pixel and $r_{i,j}$ represents the corresponding reliability of the direction. Instead of computing LRD at each pixel, most algorithms extract the LRD at discrete positions of a palmprint image. Three representative methods are commonly used to estimate the LRD of a palmprint image, including gradient-based method, discrete Fourier transform (DFT), and Gabor filter-based methods. After obtaining LRD, the reliability r of the palmprint image can be derived by the concordance of the direction vectors in the local window.

The basic idea of the gradient-based method [111] is that the ridges and valleys of a palmprint image are the black and white stripes. The LRD is determined as the orthogonal direction of the gradient phase angle, which denotes the direction of the maximum intensity change. However, creases are widely distributed in a palmprint, which severely affect the LRD estimation results of the gradient-based methods.

The Gabor filter-based method [111] applies a serial of Gabor filters to multiply the frequency spectrum of the local area. Then, it selects the direction of the Gabor filter which achieves the maximum filtering response as the LRD of the area. The Gabor filter-based method is relatively time-consuming due to its high computational complexity.

DFT [33], [48] is one of the most effective tools to estimate the LRD of a palmprint image, which assumes to use the sine wave to represent the ridge flows of the palmprint image. So the peak in the frequency domain of a local area corresponds to the central lines of the stripes in the palmprint image. Specifically, a palmprint image is divided into nonoverlapping blocks with the size of 16×16 pixels, each of which is multiplied by a Gaussian function. The DFT of the resulting images is computed. Here after, the top k likely directions of the block is determined based on the amplitude. Supposing that the ith peak in the frequency spectrum is (u_i, v_i), the ridge direction θ_i can be determined as $(v_i/u_i) - (\pi/2)$. Based on the assumption that waves corresponding to ridges form the continuous and sufficiently large clusters, a region grow algorithm is used to concentrate ridge directions of blocks to decide the LRD of the palmprint image. Fig. 15(a) shows the LRD map of the palmprint image in Fig. 13 [110].

A matched LRD-based block pair is considered as two overlapped blocks whose ridge direction distance is less than a threshold (e.g., $\pi/6$). Thus, the similarity between ridge direction maps can be estimated based on the number of matched block pairs (N_d) as $[N_d/(N_d + K)]$, where K is generally set to 900 to represent the number of the smallest matched block numbers for genuine matches [48].

2) Minutiae Points: Minutiae points are the most significant and discriminative features of high-resolution palmprint images [10], [113]–[115]. A vector of (x, y, θ) is usually used to represent a minutiae point, where (x, y) is the coordinate of the point and θ is the LRD at the point [115]. A simple and effective way to extract the minutiae point is as follows. At first, the ridges of a palmprint image are enhanced by Gabor filters with the orientation of LRD. Then, the palmprint image is binarized and thinned to obtain the skeleton ridge image. Finally, the minutiae are detected by calculating the crossing number (CN) of each pixel in the ridges. Specifically, the ridge pixels of both CN $= 1$ and CN $= 3$ are the minutiae points of the palmprint image, where the CN is defined as half of the sum of the differences between two adjacent pixels in the 8-bit neighborhood area. That is, $\mathrm{CN}(p) = (1/2)\sum_{k=1}^{8} |\mathrm{val}(p_{k\bmod 8}) - \mathrm{val}(p_{k-1})|$, where p_k is

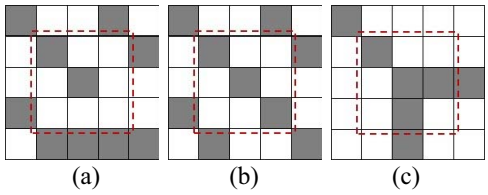

Fig. 14. CN of a center ridge pixel in a palmprint image. (a) CN(p) = 1 corresponds to a ridge ending. (b) CN(p) = 2 corresponds to a normal point. (c) CN(p) = 3 corresponds to a bifurcate.

the kth neighbor pixel of the current pixel [10]. val(.) $\in \{0, 1\}$ is the pixel value. Fig. 14 shows the procedure of minutiae points extraction, from which we see that, for a pixel with val(p) = 1, the pixel is a minutiae point if CN(p) is 1 or 3, otherwise, the pixel is an intermediate ridge point.

Due to the influence of creases, many spurious minutiae points may be detected as minutiae points. A simple way to remove the spurious minutiae points is to find out if two potential minutiae points have the same or opposite directions in a small neighboring area. In addition, since the spurious minutiae points are mainly caused by creases, Dai and Zhou [48] extracted the creases and then removed the detected minutiae if it is close to a crease. Fig. 15(c) shows the minutiae points detected in the palmprint image of Fig. 13, where the ridge endings and ridge bifurcates are marked as red and blue, respectively.

In the matching stage of minutiae point descriptors, the elements of (x, y, θ) are, respectively, compared between two minutiae points. Given two minutiae points of two palmprint images as (x_i, y_i, θ_i) and (x'_j, y'_j, θ'_j), they are considered as matched if differences between corresponding elements are less than the given tolerances [10], [33], [111]

$$\begin{aligned} &\left|x_i - x'_j\right| < \delta_x \\ &\left|y_i - y'_j\right| < \delta_y \\ &\min\left(\left|\theta_i - \theta'_j\right|, 2\pi - \left|\theta_i - \theta'_j\right|\right) < \delta_\theta \end{aligned} \tag{12}$$

where δ_x, δ_y, and δ_θ are the predefined thresholds for corresponding elements. Then, the similarity between two minutiae descriptors can be evaluated using the proportion of the matched minutiae number to the total minutiae number of two minutiae point maps.

3) Principal Lines: The principal lines are the most significant and stable features of the palmprint, which can be seen in both low-resolution and high-resolution palmprint images [48]. In a high-resolution palmprint image, the principal lines are the most three widest and longest creases. The normal creases of a palmprint image can be detected by using MFRAT, and then the Hough transform can be applied to detect the principal lines among creases [48]. Suppose $w\cos\theta + h\sin\theta = r$ be the major axis of a candidate rectangular area including a principal line, the general Hough transform is defined as follows:

$$G(\theta, r) = \int_0^H \int_0^W I_E(w, h) T\left(|r - w\cos\theta - h\sin\theta| < \frac{W}{2}\right) T(|I_D(w, h) - \theta| < \Psi) dw dh \tag{13}$$

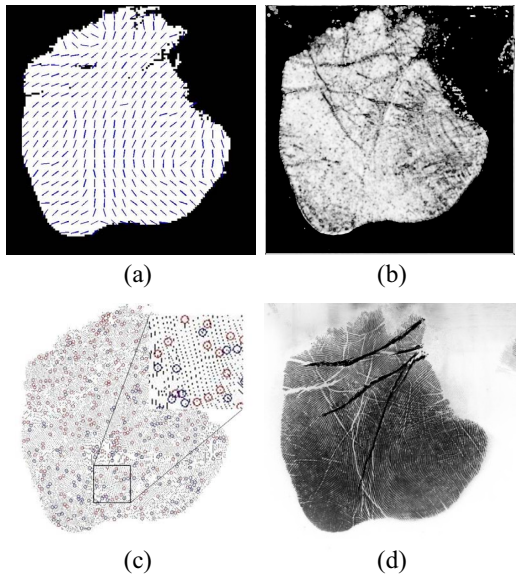

Fig. 15. Features extracted from a palmprint image. (a) LRD map. (b) Local ridge density image. (c) Minutiae point map. (d) Principal line image.

where I_E and I_D are the crease energy and crease direction maps, respectively, which are obtained by using MFRAT. W and Ψ are the thresholds of the direction and position differences, respectively. $T(c)$ equals 1 if c is true, otherwise, it is 0. So $G(\theta, r)$ is to collect the energy of a latent principal line on a possible principal direction, that is, I_D. After that, the top k peaks of parameter spaces can be obtained corresponding to k rectangular areas. The creases outside the k rectangular areas are removed from the I_E and I_D to form the principal line image. The similarity of principal line maps can be measured by the proportion of matched principal line energy in all the energy within the common area, in which two energy points are considered to be matched if they are located at the similar positions and the direction difference of them is small, e.g., $\pi/6$ [48]. Fig. 15(d) shows the principal lines extracted from the palmprint image of Fig. 13.

C. Experiments

In this section, we compare the discriminative power of different features, including the LRD, local ridge density, minutiae points, and principal lines, on a high-resolution palmprint image database.

1) High-Resolution Palmprint Image Database: The THU high-resolution palmprint database [110] consists of 1280 high-resolution palmprint images collected from 80 subjects. Each individual provided eight images from both the left and right palms. The original palmprint images are the sizes of 2040×2040 pixels and 256 grayscales with 500 ppi resolution. Fig. 16 shows four typical high-resolution palmprint images in the THU database. Up to now, the THU database is the only public high-resolution palmprint image database.

2) Palmprint Recognition Results: In experiments, the LRD, ridge density, minutiae points, and principal lines are, respectively, extracted and matched to conduct both palmprint

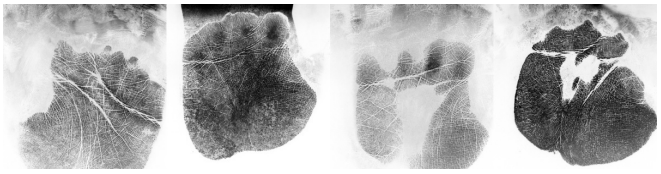

Fig. 16. Four typical high-resolution palmprint images selected from the THU palmprint database.

TABLE VI
EERs (%) OF PALMPRINT VERIFICATION AND ERROR RATES (%) OF PALMPRINT IDENTIFICATION OBTAINED BASED ON DIFFERENT FEATURES OF PALMPRINT ON THU PALMPRINT DATABASE

	EER(verification)	Error rate(identification)
Ridge direction	0.311	38.47
Ridge density	0.205	32.32
Minutiae point	0.148	28.56
Principal line	0.407	56.52

verification and palmprint identification. In palmprint verification, each palmprint image will be compared with any other samples leading to 4480 genuine matches and 814 080 impostor matches. For palmprint identification, the first four images per each subject are selected as training samples and the rest images are used as query samples. In the experiments, the palmprint images are resized to 1020×1020 pixels to improve the efficiency of the algorithms without reducing the quality. Before feature extraction, the valid palmprint area of the palmprint images are marked using [44]. After that, the palmprint images are enhanced by using [41] to improve the quality of ridge patterns. The EERs of palmprint verification and error rates of rank-1 palmprint identification obtained using different features are summarized in Table VI.

We can see from above table that the minutia point feature has higher discriminability than the other features, and the principal line has the lowest discriminability. Further, local ridge density has higher discriminability than the LRD. The possible reasons are as follows. First, because many minutia points can be detected in a full high-resolution palmprint image, which are almost the highest discriminative features of the palmprint images [48], [49]. Second, the principal lines can be extracted from both low-resolution and high-resolution palmprint images. However, many palmprint may have similar principal lines resulting in its low discriminability, and further many principal lines may not be stably extracted from high-resolution palmprint images. So the principal lines are usually worked with other features in palmprint recognition. Third, the ridge pattern flows in the same region are relatively similar among the samples so that the discriminability of ridge direction is not comparable to the local ridge density. In real-world applications, instead of using the single feature, many methods [48] usually extract and fuse multiple features for more accurate palmprint recognition.

It should be pointed out that the level-3 features can only be detected from the palmprint image with more than 500 ppi, or even 1000 ppi, which means that a high-definition scanner is required in the image capture. In addition, the level-3 features are sensitive to noise. So the level-3 features are seldom used in real-world palmprint recognition [33].

In addition, it is believed that the level-2 features generally have high discriminability than the level-1 features of the palmprint. However, with compared with low-resolution palmprint recognition, the accuracy of the high-resolution palmprint recognition is low. On the one hand, as show in Fig. 16, the high-resolution palmprint images in real-world applications are generally of poor quality. On the other hand, the level-2 features are sensitive to noise and the environments of image acquisition. In other words, the level-2 features of the palmprint are hard to be captured and to be clearly presented in high-resolution palmprint images. In addition, the wild distributions of creases produce many spurious minutiae points in high-resolution palmprint images. So the high-resolution palmprint recognition methods generally cannot accurately and stably extract the level-2 features from high-resolution palmprint images. How to accurately and robustly extract the level-2 features of the palmprint is still the challenging problem of high-resolution palmprint recognition.

V. 3-D PALMPRINT RECOGNITION

A. Features in 3-D Palmprint Image

Three-dimensional palmprint images reflect the depth information of the palmprint surfaces [99]. The local curvatures, including mean curvatures and Gaussian curvatures, can depict the surface characteristics of 3-D palmprint images. Also, the ST can characterize the structure shapes of the palmprint surfaces. Normally, the mean curvatures, Gaussian curvatures and ST form the basic features of 3-D palmprint images [116].

Three-dimensional palmprint images need to be preprocessed to crop the center area, that is, ROI, before feature extraction. The scheme described in [52] is used to extract the ROI of a 3-D palmprint image. Specifically, both the 2-D and 3-D palmprint images are captured simultaneously by using the structured-light imaging technology. With the help of user-pegs in the acquisition device, the 2-D palmprint ROI can be easily located. Since the points in the 3-D palmprint image and corresponding 2-D counterpart have one-to-one correspondences, the 3-D palmprint ROI can be directly cropped based on the coordinate system established in 2-D palmprint ROI extraction. After that, the 3-D palmprint images are basically aligned to reduce the impact of small translation and rotation introduced in data acquisition.

B. Feature Extraction of 3-D Palmprint Image

1) Mean Curvature and Gaussian Curvature: A 3-D palmprint can be considered as a surface with various convex and concave structures. Given a point of a 3-D palmprint image, any curves on the surface pass through the point have different curvatures. Among them, at least one curvature has the maximum value and one has the minimum value. Suppose the largest and smallest curvatures of the point are $c_{\max}$ and $c_{\min}$, respectively, the mean curvature (H) and Gaussian curvatures (K) are as follows [52]:

$$H = \frac{c_{\max} + c_{\min}}{2} \tag{14}$$

and

$$K = c_{\max} \times c_{\min}. \tag{15}$$

We see that the mean and Gaussian curvatures essentially depend only on the surface shape but not on the placement of the palm surface on the device. So the mean and Gaussian curvatures show high robustness to misalignment and even the deformation of the surface [52]. Thus, the mean curvature and Gaussian curvature are widely used in 3-D palmprint recognition.

A efficient way to compute the mean and Gaussian curvatures of a 3-D palmprint is based on a bank of predefined window templates. Specifically, before curvature calculation, the range data of a 3-D palmprint image is first preprocessed by using a binomial filter $S = ss^T$, where $s = (1/64)[1\ 6\ 15\ 20\ 15\ 6\ 1]^T$. Then, a set of partial derivative estimation window templates are, respectively, defined as $D_x = d_0 d_1^T$, $D_y = d_1 d_0^T$, $D_{xx} = d_0 d_2^T$, $D_{yy} = d_2 d_0^T$, and $D_{xy} = d_1 d_1^T$, where column vectors $d_i (i = 0, 1, 2)$ are given as: $d_0 = (1/7)[1\ 1\ 1\ 1\ 1\ 1\ 1]^T$, $d_1 = (1/28)[-3\ -2\ -1\ 0\ 1\ 2\ 3]$ and $d_2 = (1/84)[5\ 0\ -3\ -4\ -3\ 0\ 5]$, respectively. After that, suppose f denotes the depth of a point in a 3-D surface, the first and second order partial derivatives of $f(x, y)$ along corresponding $x(y)$ coordinate can be calculated as follows:

$$f_u(x, y) = D_u \otimes S \otimes f(x, y), (u = x, y, xx, yy, xy) \tag{16}$$

where $f_x(f_y)$ is the first order derivative of f to the $x(y)$ coordinate, $f_{xx}(f_{yy})$ is the second order derivative of f along the $x(y)$ coordinate, and f_{xy} is the second order derivate of f along the x and y coordinates, respectively. Finally, the mean and Gaussian curvatures of the 3-D image (f) can be directly obtained as follows [117]:

$$H = \frac{\left(1 + f_x^2\right) f_{yy} + \left(1 + f_y^2\right) f_{xx} - 2 f_x f_y f_{xy}}{2\left(1 + f_x^2 + f_y^2\right)^{3/2}} \tag{17}$$

and

$$K = \frac{f_{xx} f_{yy} - f_{xy}^2}{\left(1 + f_x^2 + f_x^2\right)^2}. \tag{18}$$

Based on the mean and Gaussian curvatures, several methods were proposed for 3-D palmprint recognition. For example, Zhang *et al*. [58] transformed the mean and Gaussian curvatures of a 3-D palmprint image into gray level images named as MCI and GCI, respectively. Then, the MCI and GCI were simply converted into binary images by thresholding and the bit-wise logical operations can be used in the matching stage. Comparatively, Li *et al*. [59], [60] extracted the line features of the MCI and GCI by thresholding and meanwhile calculated the competitive codes of MCI and GCI. The matching score of line features and angular distance of the competitive code planes were fused in score level in the decision making.

2) Surface Type: A 3-D palmprint image comprises various convex and concave surfaces. ST [100] can better describe the characteristics of 3-D surfaces. Table VII presents the definition of the ST based on the signs of the Gaussian and mean curvatures. It is pointed out that a special ST with $H = 0$ and $K > 0$ corresponding to nonexisting real surface shape is still used. As a result, a point in a 3-D palmprint can be classified into one of the nine STs.

TABLE VII
ST DEFINITION OF 3-D PALMPRINT IMAGES

	$K > 0$	$K = 0$	$K < 0$
$H > 0$	Peak(ST=1)	Ridge(ST=2)	Saddle ridge(ST=3)
$H = 0$	None(ST=4)	Flat(ST=5)	Minimal surface(ST=6)
$H < 0$	Pit(ST=7)	Valley(ST=8)	Saddle valley(ST=9)

The mean and Gaussian curvatures of a 3-D palmprint image obtained by using (17) and (18) are usually floats. To classify the points of a 3-D palmprint image into nine STs, the scales of H and K are quantized to determine the intervals to define the scenarios of $H = 0$ and $K = 0$, respectively. This can be simply implemented by defining two thresholding parameters ε_H and ε_K. Specifically, the mean or Gaussian curvatures are first normalized by their standard deviation as $C(i, j) = C(i, j)/2\delta$ (C represents K or H, and δ represents the standard deviation of the curvature value) and thus most curvature values will fall into the interval of $[-1, 1]$ without changing their signs. Then, two thresholds around zero can be set for both ε_H and ε_K, such as $\varepsilon_H = 0.03$ and $\varepsilon_K = 0.015$, respectively. The H and K of a point are set to 0 if it is in the range of $(-\varepsilon_H, \varepsilon_H)$ and $(-\varepsilon_K, \varepsilon_K)$, respectively [101].

ST is another significant features of 3-D palmprint images, which has been widely used in 3-D palmprint recognition. For example, Zhang *et al*. [52] proposed a 3-D palmprint recognition method based on MCI, GCI, and ST, in which the line features were extracted from MCI and GCI and then nine binary ST maps were defined for the 3-D palmprint image. The corresponding feature maps were, respectively, compared between the training and query samples and finally fused in score level. In addition, Zhang *et al*. [117] applied sparse representation on the ST vectors for 3-D palmprint recognition achieving competitive performance. They divided a 3-D palmprint image into several uniform blocks and calculated the block-wise ST histograms, which were concentrated to form a global descriptor of the 3-D palmprint. The CR-based classification scheme was used to identify a query 3-D palmprint image.

C. Experiments

In this section, we compare the performances of the state-of-the-art 3-D palmprint recognition methods on a public 3-D palmprint database. The compared methods include MCI competitive code fusing with location method (MCI_Comp) [59], MCI ordinal code method (MCI_OLOF) [117], SII orientation feature fusing with LBP method (SII_LBP) [119], MCI, GCI, and ST binarization and fusion method (MCI_GCI_ST) [52] and CR-based [117] 3-D palmprint identification methods (CR_CompCode).

1) 3-D Palmprint Image Database: The PolyU 3-D palmprint database [120] was established by Biometric Research Center of Hong Kong Polytechnic University, which designed a structured-light imaging-based device that can simultaneously capture both the 2-D and 3-D palmprint

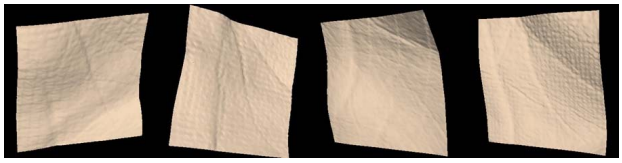

Fig. 17. Four typical 3-D palmprint images selected from the PolyU 3-D palmprint image database.

TABLE VIII
EERs (%) of Palmprint Verification and Error Rate (%) of Palmprint Identification Obtained Using Different Methods on the PolyU 3-D Palmprint Database

	EER(verification)	Error rate(identification)
MCI_Comp	0.0440	3.60
MCI_OLOF	0.0556	7.60
SII_LBP	0.0755	11.92
MCI_GCI_ST	0.0928	9.40
CR_CompCode	-	1.00

images. Of them, the PolyU 3-D palmprint database is used in this experiment, which has 8000 3-D palmprint images collected from 200 individuals, including 136 males and 64 females. The palmprint images in the database were collected in two sessions with an interval of around one month. Ten palmprint images were captured from each palm of an individual in each session and thus 20 palmprint images were captured from a palm. Fig. 17 shows the typical 3-D palmprint images selected from the database.

2) Palmprint Recognition Results: In the experiments, we conduct both palmprint verification and identification to test the performances of different 3-D palmprint recognition methods on the PolyU 3-D palmprint database. The procedures of palmprint verification and identification are detailed in Section II-D. Particularly, the total number of matches is 31 996 000, and of which 76 000 are genuine matches and 31 920 000 are impostor matches. It is pointed out that the CR_CompCode method is based on the linear representation which needs defining a dictionary set by using all training samples from all palms. So it is infeasible to do the one-to-one comparison. EERs obtained using different methods are listed in Table VIII.

In palmprint identification, the palmprint images captured in the first session are used as the training samples and the images collected in the second session are used as the query samples. The error rates of rank-1 palmprint identification obtained using different methods are summarized in Table VIII.

From the comparative results, we can draw the following observations. At first, the orientation features, such as in the MCI_Comp and MCI_OLOF methods, extracted from MCI are more discriminative than the line features by simple thresholding, such as the MCI_GCI_ST method. The main reason is that MCI can better reflect the texture feature of a palmprint. So the orientation features can be captured by the competitive code and OLOF methods. Second, the MCI_Comp outperforms the MCI_OLOF method. It is because that the competitive code is more discriminative than the OLOF extracted from MCI, which is consistent with the conclusion of Section II. Third, the CR_CompCode method achieves much higher accuracy than the other methods in 3-D palmprint identification, which show the effectiveness of the ST-based features of 3-D palmprint. In addition, block-based histogram of ST shows high robustness to mere misalignments of 3-D palmprint images.

It is recognized that the texture feature map, that is, MCI, recovered from the 3-D palmprint is of gray-level and depicts the level-1 features of the palmprint. Therefore, the conventional palmprint recognition methods, such as the competitive code and ordinal code methods, can be directly used to extract the orientation features of the 3-D palmprint based on the MCI. In addition, the ST reflects the basic surface structures of the 3-D palmprint. Therefore, the representative 3-D palmprint recognition methods usually combine the 2-D texture-based features and the 3-D ST-based features for 3-D palmprint recognition.

In addition, 3-D palmprint images are captured with contact-based device and thereby are well aligned. Furthermore, there is no doubt that a 3-D palmprint image depends on the changes of a palm surface, and thereby it shows excellent robustness to illumination variations. That is why the state-of-the-art methods can achieve high accuracies in 3-D palmprint recognition. Now, contactless palmprint recognition has attracted a wide range of attentions due to its high user-acceptance. In the future, developing contactless 3-D palmprint recognition appears to be an interesting and meaningful direction.

VI. Conclusion

In this paper, we summarize the feature extraction and matching for all types of palmprint images. First, we use a unified framework to group the palmprint images into four categories, including contact-based palmprint images, contactless palmprint images, high-resolution palmprint images, and 3-D palmprint images. Then, for each category of the palmprint images, we introduce the intrinsic features of them, and further analyze the motivation and theory of state-of-the-art methods on feature extraction and recognition. Finally, we compare the efficiency of different methods on the widely used palmprint databases, and also offer the crossing comparisons among different types of palmprint recognition.

Over the past few years, contact-based palmprint recognition has reached a high accuracy. Comparatively, the contactless palmprint recognition cannot obtain the comparable accuracy because the contactless palmprint images are generally captured under free environments with using an ordinary camera. However, contactless palmprint recognition has high acceptability because of its loose image acquisition condition. Therefore, the further research on palmprint recognition should focus on the field of contactless-based palmprint recognition. It has been verified that the deep-learning methods achieve encouraging performance on contactless palmprint recognition, which validates the feasibility of developing the deep-learning-based palmprint recognition methods. Further, the 3-D palmprint images are also captured under contact-based device leading to a high accuracy of 3-D palmprint recognition. Therefore, it appears to be interesting and meaningful to explore the contactless 3-D palmprint recognition in the future. In addition,

automatic high-resolution palmprint recognition serves as an important source of real-world high-security applications, e.g., forensic usage. However, the level-2 features of the palmprint are hard to be accurately extracted from high-resolution palmprint images because of the poor quality of the images and their sensitiveness to the noise. Existing works demonstrate that it is normally difficult to achieve acceptable performance based on only one kind of level-2 features. Therefore, it is feasible to combine different level-2 features to boost the accuracy of high-resolution palmprint recognition.

REFERENCES

[1] D. Zhang, *Automated Biometrics: Technologies and Systems*. New York, NY, USA: Springer, 2013.

[2] A. K. Jain, A. Ross, and S. Prabhakar, "An introduction to biometric recognition," *IEEE Trans. Circuits Syst. Video Technol.*, vol. 14, no. 1, pp. 4–20, Jan. 2004.

[3] D.-S. Huang, W. Jia, and D. Zhang, "Palmprint verification based on principal lines," *Pattern Recognit.*, vol. 41, no. 4, pp. 1316–1328, Apr. 2008.

[4] D. Zhang and W. Shu, "Two novel characteristics in palmprint verification: Datum point invariance and line feature matching," *Pattern Recognit.*, vol. 32, no. 4, pp. 691–702, 1999.

[5] F. Chen, X. Huang, and J. Zhou, "Hierarchical minutiae matching for fingerprint and palmprint identification," *IEEE Trans. Image Process.*, vol. 22, no. 12, pp. 4964–4971, Dec. 2013.

[6] Y. Ding, D. Zhuang, and K. Wang, "A study of hand vein recognition method," in *Proc. IEEE Int. Conf. Mechatronics Autom.*, 2005, pp. 2106–2110.

[7] X. Wang and X. Tang, "A unified framework for subspace face recognition," *IEEE Trans. Pattern Anal. Mach. Intell.*, vol. 26, no. 9, pp. 1222–1228, Sep. 2004.

[8] M. I. Ahmad, W. L. Woo, and S. Dlay, "Non-stationary feature fusion of face and palmprint multimodal biometrics," *Neurocomputing*, vol. 177, pp. 49–61, Feb. 2016.

[9] J. Daugman, A. K. Jain, R. Bolle, and S. Pankanti, "Recognizing persons by their Iris patterns," *Inf. Security Tech. Rep.*, vol. 3, no. 1, pp. 33–39, 1998.

[10] D. Maltoni, D. Maio, A. K. Jain, and S. Prabhakar, *Handbook of Fingerprint Recognition*. London, U.K.: Springer-Verlag, 2009.

[11] Q. Zheng, A. Kumar, and G. Pan, "Suspecting less and doing better: New insights on palmprint identification for faster and more accurate matching," *IEEE Trans. Inf. Forensics Security*, vol. 11, no. 3, pp. 633–641, Mar. 2016.

[12] A. Kong, D. Zhang, and M. Kamel, "A survey of palmprint recognition," *Pattern Recognit.*, vol. 42, no. 7, pp. 1408–1418, Jul. 2009.

[13] K. Tiwari, D. K. Arya, G. S. Badrinath, and P. Gupta, "Designing palmprint based recognition system using local structure tensor and force field transformation for human identification," *Neurocomputing*, vol. 116, pp. 222–230, Sep. 2013.

[14] S. Chakraborty, I. Bhattacharya, and A. Chatterjee, "A palmprint based biometric authentication system using dual tree complex wavelet transform," *Measurement*, vol. 46, no. 10, pp. 4179–4188, 2013.

[15] X. Wang, J. Liang, and M. Wang, "On-line fast palmprint identification based on adaptive lifting wavelet scheme," *Knowl.-Based Syst.*, vol. 42, pp. 68–73, Apr. 2013.

[16] X. Wu, D. Zhang, and K. Wang, "Fisherpalms based palmprint recognition," *Pattern Recognit. Lett.*, vol. 24, no. 15, pp. 2829–2838, 2003.

[17] D. Zhao, X. Pan, X. Luo, and X. Gao, "Palmprint recognition based on deep learning," in *Proc. ICWMMN*, 2015, pp. 214–216.

[18] S. Minaee and Y. Wang, "Palmprint recognition using deep scattering convolutional network," *arXiv preprint arXiv:1603.09027*, 2016. [Online]. Available: https://arxiv.org/abs/1603.09027

[19] L. Leng and A. B. J. Teoh, "Alignment-free row-co-occurrence cancelable palmprint fuzzy vault," *Pattern Recognit.*, vol. 48, no. 7, pp. 2290–2303, 2015.

[20] S. Kanchana and G. Balakrishnan, "Palm-print pattern matching based on features using Rabin–Karp for person identification," *Sci. World J.*, vol. 2015, pp. 1–9, Oct. 2015. [Online]. Available: https://www.hindawi.com/journals/tswj/2015/382697/

[21] X. Wu, D. Zhang, and K. Wang, "Palm line extraction and matching for personal authentication," *IEEE Trans. Syst., Man, Cybern. A, Syst., Humans*, vol. 36, no. 5, pp. 978–987, Sep. 2006.

[22] F. Yue, B. Li, M. Yu, and J. Wang, "Hashing based fast palmprint identification for large-scale databases," *IEEE Trans. Inf. Forensics Security*, vol. 8, no. 5, pp. 769–778, May 2013.

[23] V. Roux, S. Aoyama, K. Ito, and T. Aoki, "Performance improvement of phase-based correspondence matching for palmprint recognition," in *Proc. IEEE Conf. Comput. Vis. Pattern Recognit.*, 2014, pp. 70–77.

[24] S. Lin and Y. Tai, "A combination recognition method of palmprint and palm vein based on gray surface matching," in *Proc. Int. Congr. Image Signal Process.*, 2015, pp. 567–571.

[25] Y. Xu, L. Fei, and D. Zhang, "Combining left and right palmprint images for more accurate personal identification," *IEEE Trans. Image Process.*, vol. 24, no. 2, pp. 549–559, Feb. 2015.

[26] D. Hong, W. Liu, J. Su, Z. Pan, and G. Wang, "A novel hierarchical approach for multispectral palmprint recognition," *Neurocomputing*, vol. 151, Part. 1, pp. 511–521, Mar. 2015.

[27] D. Zhang, Z. Guo, G. Lu, L. Zhang, and W. Zuo, "An online system of multispectral palmprint verification," *IEEE Trans. Instrum. Meas.*, vol. 59, no. 2, pp. 480–490, Feb. 2010.

[28] A. Kumar and S. Shekhar, "Personal identification using multibiometrics rank-level fusion," *IEEE Trans. Syst., Man, Cybern. C, Appl. Rev.*, vol. 41, no. 5, pp. 743–752, Sep. 2011.

[29] J. Malik, D. Girdhar, and R. Dahiya, "Accuracy improvement in palmprint authentication system," *Int. J. Image Graph. Signal Process.*, vol. 7, no. 4, pp. 51–59, 2015.

[30] D. Zhang, W. Zuo, and F. Yue, "A comparative study of palmprint recognition algorithms," *ACM Comput. Surveys*, vol. 44, no. 1, pp. 2–38, Jan. 2012.

[31] W. Jia, D.-S. Huang, and D. Zhang, "Palmprint verification based on robust line orientation code," *Pattern Recognit.*, vol. 41, no. 5, pp. 1504–1513, 2008.

[32] D. Zhang, W.-K. Kong, J. You, and L. M. Wong, "Online palmprint identification," *IEEE Trans. Pattern Anal. Mach. Intell.*, vol. 25, no. 9, pp. 1041–1050, Sep. 2003.

[33] A. K. Jain and J. Feng, "Latent palmprint matching," *IEEE Trans. Pattern Anal. Mach. Intell.*, vol. 31, no. 6, pp. 1032–1047, Jun. 2009.

[34] A. W.-K. Kong and D. Zhang, "Competitive coding scheme for palmprint verification," in *Proc. Int. Conf. Pattern Recognit. (ICPR)*, 2004, pp. 520–523.

[35] A. Kong, D. Zhang, and M. Kamel, "Palmprint identification using feature-level fusion," *Pattern Recognit.*, vol. 39, no. 3, pp. 478–487, 2006.

[36] Z. Sun, T. Tan, Y. Wang, and S. Li, "Ordinal palmprint represention for personal identification [represention read representation]," in *Proc. IEEE Conf. Comput. Vis. Pattern Recognit.*, vol. 1, Jun. 2005, pp. 279–284.

[37] Z. Guo, D. Zhang, L. Zhang, and W. Zuo, "Palmprint verification using binary orientation co-occurrence vector," *Pattern Recognit. Lett.*, vol. 30, no. 13, pp. 1219–1227, 2009.

[38] D. Tamrakar and P. Khanna, "Palmprint verification with XOR-SUM code," *Signal Image Video Process.*, vol. 9, no. 3, pp. 535–542, 2015.

[39] G. K. O. Michael, T. Connie, and A. B. J. Teoh, "Touch-less palm print biometrics: Novel design and implementation," *Image Vis. Comput.*, vol. 26, no. 12, pp. 1551–1560, 2008.

[40] A. Morales, M. A. Ferrer, and A. Kumar, "Towards contactless palmprint authentication," *IET Comput. Vis.*, vol. 5, no. 6, pp. 407–416, Nov. 2011.

[41] A. S. Parihar *et al.*, "Point based features for contact-less palmprint images," in *Proc. IEEE Int. Conf. Technol. Homeland Security (HST)*, 2013, pp. 165–170.

[42] M. Choraś and R. Kozik, "Contactless palmprint and knuckle biometrics for mobile devices," *Pattern Anal. Appl.*, vol. 15, no. 1, pp. 73–85, 2012.

[43] X. Wu and Q. Zhao, "Deformed palmprint matching based on stable regions," *IEEE Trans. Image Process.*, vol. 24, no. 12, pp. 4978–4989, Dec. 2015.

[44] X. Wu, Q. Zhao, and W. Bu, "A SIFT-based contactless palmprint verification approach using iterative RANSAC and local palmprint descriptors," *Pattern Recognit.*, vol. 47, no. 10, pp. 3314–3326, 2014.

[45] L. Leng, M. Li, C. Kim, and X. Bi, "Dual-source discrimination power analysis for multi-instance contactless palmprint recognition," *Multimedia Tools Appl.*, vol. 76, no. 1, pp. 333–354, 2017.

[46] M. Aykut and M. Ekinci, "AAM-based palm segmentation in unrestricted backgrounds and various postures for palmprint recognition," *Pattern Recognit. Lett.*, vol. 34, no. 9, pp. 955–962, 2013.

[47] J. Funada *et al.*, "Feature extraction method for palmprint considering elimination of creases," in *Proc. Int. Conf. Pattern Recognit. (ICPR)*, 1998, pp. 1849–1854.

[48] J. Dai and J. Zhou, "Multifeature-based high-resolution palmprint recognition," *IEEE Trans. Pattern Anal. Mach. Intell.*, vol. 33, no. 5, pp. 945–957, May 2011.

[49] J. Dai, J. Feng, and J. Zhou, "Robust and efficient ridge-based palmprint matching," *IEEE Trans. Pattern Anal. Mach. Intell.*, vol. 34, no. 8, pp. 1618–1632, Aug. 2012.

[50] E. Liu, A. K. Jain, and J. Tian, "A coarse to fine minutiae-based latent palmprint matching," *IEEE Trans. Pattern Anal. Mach. Intell.*, vol. 35, no. 10, pp. 2307–2322, Oct. 2013.

[51] O. Nibouche and J. Jiang, "Palmprint matching using feature points and SVD factorisation," *Digit. Signal Process.*, vol. 23, no. 4, pp. 1154–1162, 2013.

[52] D. Zhang, G. Lu, W. Li, L. Zhang, and N. Luo, "Palmprint recognition using 3-D information," *IEEE Trans. Syst., Man, Cybern. C, Appl. Rev.*, vol. 39, no. 5, pp. 505–519, Sep. 2009.

[53] W. Li, L. Zhang, D. Zhang, G. Lu, and J. Yan, "Efficient joint 2D and 3D palmprint matching with alignment refinement," in *Proc. IEEE Conf. Comput. Vis. Pattern Recognit. (CVPR)*, 2010, pp. 795–801.

[54] Q. Zheng, A. Kumar, and G. Pan, "A 3D feature descriptor recovered from a single 2D palmprint image," *IEEE Trans. Pattern Anal. Mach. Intell.*, vol. 38, no. 6, pp. 1272–1279, Jun. 2016.

[55] W. Li, D. Zhang, G. Lu, and N. Luo, "A novel 3-D palmprint acquisition system," *IEEE Trans. Syst., Man, Cybern. A, Syst., Humans*, vol. 42, no. 2, pp. 443–452, Mar. 2012.

[56] A. Iula and D. Nardiello, "Three-dimensional ultrasound palmprint recognition using curvature methods," *J. Electron. Imag.*, vol. 25, no. 3, 2016, Art. no. 033009.

[57] L. Fei *et al.*, "Combining enhanced competitive code with compacted ST for 3D palmprint recognition," in *Proc. Asian Conf. Pattern Recognit.*, 2017, pp. 512–517.

[58] D. Zhang, G. Lu, W. Li, L. Zhang, and N. Luo, "Three dimensional palmprint recognition using structured light imaging," in *Proc. IEEE Int. Conf. Biometrics Theory Appl. Syst.*, 2009, pp. 1–6.

[59] W. Li, D. Zhang, L. Zhang, G. Lu, and J. Yan, "3-D palmprint recognition with joint line and orientation features," *IEEE Trans. Syst., Man, Cybern. C, Appl. Rev.*, vol. 41, no. 2, pp. 274–279, Mar. 2011.

[60] W. Li, L. Zhang, and D. Zhang, "Three dimensional palmprint recognition," in *Proc. IEEE Int. Conf. Syst. Man Cybern.*, 2009, pp. 4847–4852.

[61] (2005). *CASIA Palmprint Image Database*. [Online]. Available: http://biometrics.idealtest.org/

[62] P. Xinrong, T. Yangmeng, and W. Jiaqiang, "A survey of palmprint feature extraction algorithms," in *Proc. Int. Conf. Intell. Syst. Design Eng. Appl.*, 2013, pp. 57–63.

[63] (2010). *PolyU Palmprint Database (Version 2.0), Multispectral Palmprint Database*. [Online]. Available: http://www.comp.polyu.edu.hk/biometrics/

[64] Q. Dai, N. Bi, D. Huang, D. Zhang, and F. Li, "M-band wavelets application to palmprint recognition based on texture features," in *Proc. Int. Conf. Image Process.*, 2004, pp. 893–896.

[65] H. Imtiaz and S. A. Fattah, "A wavelet-based dominant feature extraction algorithm for palm-print recognition," *Digital Signal Process.*, vol. 23, no. 1, pp. 244–258, 2013.

[66] L. Shen, W. Wu, S. Jia, and Z. Guo, "Coding 3D Gabor features for hyperspectral palmprint recognition," in *Proc. Int. Conf. Med. Biometrics*, 2014, pp. 169–173.

[67] G. S. Badrinath and P. Gupta, "Palmprint based recognition system using phase-difference information," *Future Gener. Comput. Syst.*, vol. 28, no. 1, pp. 287–305, 2012.

[68] W. Jia, R.-X. Hu, Y.-K. Lei, Y. Zhao, and J. Gui, "Histogram of oriented lines for palmprint recognition," *IEEE Trans. Syst., Man, Cybern., Syst.*, vol. 44, no. 3, pp. 385–395, Mar. 2014.

[69] W. Li, L. Zhang, D. Zhang, and J. Yan, "Principal line based ICP alignment For palmprint verification," in *Proc. Int. Conf. Image Process. (ICIP)*, 2009, pp. 1961–1964.

[70] M. Aykut and M. Ekinci, "Developing a contactless palmprint authentication system by introducing a novel ROI extraction method," *Image Vis. Comput.*, vol. 40, pp. 65–74, Aug. 2015.

[71] C.-C. Han, H. Cheng, C. Lin, and K. Fan, "Personal authentication using palm-print features," *Pattern Recognit.*, vol. 36, no. 2, pp. 371–381, 2003.

[72] X. Wu, D. Zhang, K. Wang, and B. Huang, "Palmprint classification using principal lines," *Pattern Recognit.*, vol. 37, no. 10, pp. 1987–1998, 2004.

[73] L. Liu, D. Zhang, and J. You, "Detecting wide lines using isotropic nonlinear filtering," *IEEE Trans. Image Process.*, vol. 16, no. 6, pp. 1584–1595, Jun. 2007.

[74] R. Raghavendra and C. Busch, "Novel image fusion scheme based on dependency measure for robust multispectral palmprint recognition," *Pattern Recognit.*, vol. 47, no. 6, pp. 2205–2221, 2014.

[75] S. Kanchana and G. Balakrishnan, "A novel Gaussian measure curvelet based feature segmentation and extraction for palmprint images," *Indian J. Sci. Technol.*, vol. 8, no. 15, pp. 1–7, 2015.

[76] L. Zhang and H. Li, "Encoding local image patterns using Riesz transforms: With applications to palmprint and Finger–Knuckle-print recognition," *Image Vis. Comput.*, vol. 30, no. 12, pp. 1043–1051, 2012.

[77] T. S. Lee, "Image representation using 2D Gabor wavelets," *IEEE Trans. Pattern Anal. Mach. Intell.*, vol. 18, no. 10, pp. 959–971, Oct. 1996.

[78] J. H. V. Deemter and J. M. H. D. Buf, "Simultaneous detection of lines and edges using compound Gabor filters," *Int. J. Pattern Recognit. Artif. Intell.*, vol. 14, no. 6, pp. 757–777, 2000.

[79] M. D. Bounneche, L. Boubchir, A. Bouridane, B. Nekhoul, and A. Ali-Chérif, "Multi-spectral palmprint recognition based on oriented multiscale log-Gabor filters," *Neurocomputing*, vol. 205, pp. 274–286, Sep. 2016.

[80] P. S. Wu and M. Li, "Pyramid edge detection based on stack filter," *Pattern Recognit. Lett.*, vol. 18, no. 3, pp. 239–248, 1997.

[81] W. Jia *et al.*, "Palmprint recognition based on complete direction representation," *IEEE Trans. Image Process.*, vol. 26, no. 9, pp. 4483–4498, Sep. 2017.

[82] W. Zuo, Z. Lin, Z. Guo, and D. Zhang, "The multiscale competitive code via sparse representation for palmprint verification," in *Proc. IEEE Conf. Comput. Vis. Pattern Recognit. (CVPR)*, 2010, pp. 2265–2272.

[83] L. Fei, Y. Xu, W. Tang, and D. Zhang, "Double-orientation code and nonlinear matching scheme for palmprint recognition," *Pattern Recognit.*, vol. 49, pp. 89–101, Jan. 2016.

[84] F. Xue, W. Zuo, K. Wang, and D. Zhang, "A performance evaluation of filter design and coding schemes for palmprint recognition," in *Proc. Int. Conf. Pattern Recognit. (ICPR)*, 2008, pp. 1–4.

[85] L. Zhang, H. Li, and J. Niu, "Fragile bits in palmprint recognition," *IEEE Signal Process. Lett.*, vol. 19, no. 10, pp. 663–666, Oct. 2012.

[86] Y. Xu, L. Fei, J. Wen, and D. Zhang, "Discriminative and robust competitive code for palmprint recognition," *IEEE Trans. Syst., Man, Cybern., Syst.*, vol. 48, no. 2, pp. 232–241, Feb. 2018.

[87] L. Fei, Y. Xu, and D. Zhang, "Half-orientation extraction of palmprint features," *Pattern Recognit. Lett.*, vol. 69, pp. 35–41, Jan. 2016.

[88] L. Fei, B. Zhang, Y. Xu, and L. Yan, "Palmprint recognition using neighboring direction indicator," *IEEE Trans. Human-Mach. Syst.*, vol. 46, no. 6, pp. 787–798, Dec. 2016.

[89] L. Fei, J. Wen, Z. Zhang, K. Yan, and Z. Zhong, "Local multiple directional pattern of palmprint image," in *Proc. Int. Conf. Pattern Recognit. (ICPR)*, 2016, pp. 3013–3018.

[90] Z. Guo, W. Zuo, L. Zhang, and D. Zhang, "A unified distance measurement for orientation coding in palmprint verification," *Neurocomputing*, vol. 73, nos. 4–6, pp. 994–950, 2010.

[91] Z. Sun, L. Wang, and T. Tan, "Ordinal feature selection for iris and palmprint recognition," in *Proc. Int. Conf. Pattern Recognit. (ICPR)*, 2014, pp. 1–4.

[92] L. Fei, Y. Xu, B. Zhang, X. Fang, and J. Wen, "Low-rank representation integrated with principal line distance for contactless palmprint recognition," *Neurocomputing*, vol. 218, pp. 264–275, Dec. 2016.

[93] L. Zhang, L. Li, A. Yang, Y. Shen, and M. Yang, "Towards contactless palmprint recognition: A novel device, a new benchmark, and a collaborative representation based identification approach," *Pattern Recognit.*, vol. 69, pp. 199–212, Sep. 2007.

[94] T. Ojala, M. Pietikainen, and T. Maenpaa, "Multiresolution gray-scale and rotation invariant texture classification with local binary patterns," *IEEE Trans. Pattern Anal. Mach. Intell.*, vol. 24, no. 7, pp. 971–987, Jul. 2002.

[95] L. Fei, Y. Xu, S. Teng, W. Zhang, and X. Fang, "Local orientation binary pattern with use for palmprint recognition," in *Proc. Chin. Conf. Biometric Recognit.*, 2017, pp. 213–220.

[96] Y.-T. Luo *et al.*, "Local line directional pattern for palmprint recognition," *Pattern Recognit.*, vol. 50, pp. 26–44, Feb. 2016.

[97] D. G. Lowe, "Distinctive image features from scale-invariant keypoints," *Int. J. Comput. Vis.*, vol. 60, no 2, pp. 91–110, 2004.

[98] (2006). *IITD Touchless Palmprint Database (Version1.0)*. [Online]. Available: http://www4.comp.polyu.edu.hk/csajaykr/IITD/Database_Palm.htm

[99] Q. Zhao, W. Bu, and X. Wu, "SIFT-based image alignment for contactless palmprint verification," in *Proc. Internal Conf. Biometrics*, 2013, pp. 1–6.
[100] G. Hetzel, B. Leibe, P. Levi, and B. Schiele, "3D object recognition from range images using local feature histograms," in *Proc. IEEE Conf. Comput. Vis. Pattern Recognit. (CVPR)*, 2001, pp. II-394–II-399.
[101] T. Jabid, M. H. Kabir, and O. Chae, "Robust facial expression recognition based on local directional pattern," *ETRI J.*, vol. 32, no. 5, pp. 784–794, 2010.
[102] F. Zhong and J. Zhang, "Face recognition with enhanced local directional patterns," *Neurocomputing*, vol. 119, pp. 375–384, Nov. 2013.
[103] A. R. Rivera, J. R. Castillo, and O. O. Chae, "Local directional number pattern for face analysis: Face and expression recognition," *IEEE Trans. Image Process.*, vol. 22, no. 5, pp. 1740–1752, May 2013.
[104] (2011). *GPDS Palmprint Image Database*. [Online]. Available: http://www.gpds.ulpgc.es
[105] A. Krizhevsky, I. Sutskever, and G. E. Hinton, "ImageNet classification with deep convolutional neural networks," in *Proc. Neural Inf. Process. Syst. (NIPS)*, 2012, pp. 1097–1105.
[106] K. Simonyan and A. Zisserman, "Very deep convolutional networks for large-scale image recognition," *arXiv preprintarXiv:1409.1556*, 2014.
[107] K. He, X. Zhang, S. Ren, and J. Sun, "Deep residual learning for image recognition," in *Proc. IEEE Conf. Comput. Vis. Pattern Recognit. (CVPR)*, 2016, pp. 770–778.
[108] C. Szegedy, V. Vanhoucke, S. Ioffe, and J. Shlens, "Rethinking the inception architecture for computer vision," *arXiv preprint arXiv:1512.00567*, 2015.
[109] O. Russakovsky *et al.*, "ImageNet large scale visual recognition challenge," *Int. J. Comput. Vis.*, vol. 115, no. 3, pp. 211–252, 2015.
[110] (2012). *THU 500PPI Palmprint Database*. [Online]. Available: http://ivg.au.tsinghua.edu.cn/
[111] A. K. Jain, S. Prabhakar, and L. Hong, "A multichannel approach to fingerprint classification," *IEEE Trans. Pattern Anal. Mach. Intell.*, vol. 21, no. 4, pp. 348–359, Apr. 1999.
[112] D. Wan and J. Zhou, "Fingerprint recognition using model-based density map," *IEEE Trans. Image Process.*, vol. 15, no. 6, pp. 1690–1696, Jun. 2006.
[113] A. K. Jian, J. Feng, A. Nagar, and K. Nandakumar, "On matching latent fingerprint," in *Proc. IEEE Conf. Comput. Vis. Pattern Recognit. Workshops (CVPRW)*, 2008, pp. 1–8.
[114] R. Cappelli, M. Ferrara, and D. Maio, "A fast and accurate palmprint recognition system based on minutiae," *IEEE Trans. Syst., Man, Cybern. B, Cybern.*, vol. 42, no. 3, pp. 956–962, Jun. 2012.
[115] K. Karu and A. K. Jain, "Fingerprint classification," *Pattern Recognit.*, vol. 29, no. 3, pp. 389–404, 1996.
[116] P. J. Besl and R. C. Jain, "Segmentation through variable-order surface fitting," *IEEE Trans. Pattern Anal. Mach. Intell.*, vol. 10, no. 2, pp. 167–192, Mar. 1988.
[117] L. Zhang, Y. Shen, H. Li, and J. Lu, "3D palmprint identification using block-wise features and collaborative representation," *IEEE Trans. Pattern Anal. Mach. Intell.*, vol. 37, no. 8, pp. 1730–1736, Aug. 2015.
[118] M. Liu and L. Li, "Cross-correlation based binary image registration for 3D palmprint recognition," in *Proc. IEEE Int. Conf. Signal Process.*, 2012, pp. 1597–1600.
[119] B. Yang, X. Wang, J. Yao, and X. Yang, "Efficient local representation for three-dimensional palmprint recognition," *J. Electron. Imag.*, vol. 22, no. 4, 2013, Art. no. 043040.
[120] (2008). *PolyU 3D Palmprint Database*. [Online]. Available: http://www4.comp.polyu.edu.hk/biometrics/

Lunke Fei (M'17) received the B.S. degree in computer science and technology and the M.S. degree in computer application technology from East China Jiaotong University, Nanchang, China, in 2004 and 2007, respectively, and the Ph.D. degree in computer science and technology from the Harbin Institute of Technology, Harbin, China, in 2016.

He is currently an Associate Professor with the School of Computer Science and Technology, Guangdong University of Technology, Guangzhou, China. His current research interests include biometrics, pattern recognition, image processing, and machine learning.

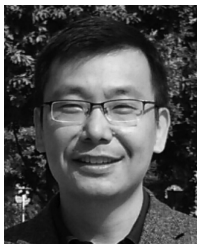

Guangming Lu received the B.S. degree in electrical engineering, the master's degree in control theory and control engineering, and the Ph.D. degree in computer science and engineering from the Harbin Institute of Technology (HIT), Harbin, China, in 1998, 2000, and 2005, respectively.

He was a Postdoctoral Fellow with Tsinghua University, Beijing, China, from 2005 to 2007. He is currently a Professor with the Shenzhen Medical Biometrics Perception and Analysis Engineering Laboratory, HIT (Shenzhen), Shenzhen, China. His current research interests include pattern recognition, image processing, and automated biometric technologies and applications.

Wei Jia (M'09) received the B.Sc. degree in informatics from Central China Normal University, Wuhan, China, in 1998, the M.Sc. degree in computer science from the Hefei University of Technology, Hefei, China, in 2004, and the Ph.D. degree in pattern recognition and intelligence system from the University of Science and Technology of China, Hefei, in 2008.

He has been a Research Assistant and Associate Professor with the Hefei Institutes of Physical Science, Chinese Academy of Science, Beijing, China, from 2008 to 2016. He is currently a Research Associate Professor with the School of Computer and Information, Hefei University of Technology. His current research interests include computer vision, biometrics, pattern recognition, image processing, and machine learning.

Shaohua Teng received the Ph.D. degree in industry engineering from the Guangdong University of Technology, Guangzhou, China, in 2008.

He is currently a Professor with the Guangdong University of Technology. He has applied for six patents on his inventions. He has authored 300 papers on computer magazines and international conferences and two books. His current research interests include big data, network security, cooperative work, machine learning, and statistical pattern recognition.

Prof. Teng was a recipient of the Provincial Science and Technology Award in 2012 and the Guangdong Outstanding Teacher in 2015.

David Zhang (F'08) received the graduation degree in computer science from Peking University, Beijing, China, in 1974 and the M.Sc. degree in computer science and the Ph.D. degree in computer engineering from the Harbin Institute of Technology (HIT), Harbin, China, in 1982 and 1985, respectively.

From 1986 to 1988, he was a Postdoctoral Fellow with Tsinghua University, Beijing, and an Associate Professor with the Academia Sinca, Beijing. He is currently the Head of the Department of Computing, and the Chair Professor with Hong Kong Polytechnic University, Hong Kong, where he is the Founding Director of the Biometrics Technology Centre supported by the Hong Kong SAR Government in 1998. He also serves as a Visiting Chair Professor with Tsinghua University, and an Adjunct Professor with Peking University, Shanghai Jiao Tong University, Shanghai, China, HIT, and the University of Waterloo. He has authored over ten books and 200 journal papers.

Prof. Zhang is the Founder and an Editor-in-Chief of the *International Journal of Image and Graphics*, the Book Editor of the Springer International Series on Biometrics, an Organizer of the International Conference on Biometrics Authentication, an Associate Editor of over ten international journals, including the IEEE TRANSACTIONS and *Pattern Recognition*. He is a Croucher Senior Research Fellow, the Distinguished Speaker of the IEEE Computer Society, and a fellow of the International Association for Pattern Recognition.